Geochemistry Geophysics Geosystems G3
AN ELECTRONIC JOURNAL OF THE EARTH SCIENCES
Published by AGU and the Geochemical Society

Article
Volume 7, Number 7
12 July 2006
Q07O02, doi:10.1029/2006GC001242
ISSN: 1525-2027

Click Here for Full Article

Hydrothermal recharge and discharge guided by basement outcrops on 0.7–3.6 Ma seafloor east of the Juan de Fuca Ridge: Observations and numerical models

M. Hutnak
Department of Earth Sciences, University of California, Santa Cruz, 1156 High Street, Santa Cruz, California 95064, USA (mhutnak@pmc.ucsc.edu)

A. T. Fisher
Department of Earth Sciences, University of California, Santa Cruz, 1156 High Street, Santa Cruz, California 95064, USA

Institute for Geophysics and Planetary Physics, University of California, Santa Cruz, 1156 High Street, Santa Cruz, California 95064, USA

L. Zühlsdorff and V. Spiess
Department of Geosciences, University of Bremen, P.O. Box 33 04 40, D-28334 Bremen, Germany

P. H. Stauffer and C. W. Gable
Earth and Environmental Sciences Division, Los Alamos National Laboratory, TA-3, SM31, MS-c306, Los Alamos, New Mexico 87545, USA

[1] The nature of ridge-flank hydrothermal circulation guided by basement outcrops protruding through thick sediments is constrained on the eastern flank of the Juan de Fuca Ridge using combined bathymetric, seismic, and thermal observations and analytical and numerical calculations of coupled fluid-heat flow. Observational data near the western edge of the survey area indicate that young, cool hydrothermal fluids circulate rapidly through upper basement, probably both across-strike and along-strike of dominant structural trends. Data from the eastern end of survey coverage (Second Ridge (SR)) indicate that upper basement is regionally nearly isothermal. A small number of basement outcrops in this area host focused hydrothermal discharge, as do additional basement outcrops to the north and south of the SR area. Numerical models of individual recharging and discharging outcrops, patterned after the Baby Bare and Grizzly Bare outcrops, suggest that local convection alone cannot explain observed patterns of seafloor heat flux near these features. Forced-flow simulations show that reasonable rates of hydrothermal recharge and discharge, inferred from independent observations, can explain nearby seafloor heat flux, provided that upper basement permeability within and near the outcrops falls within a range of 10^{-13} to 10^{-11} m^2. Free-flow simulations of fluid circulation between paired outcrops separated by 50 km, as are Baby Bare and Grizzly Bare outcrops, are most consistent with observations when regional basement permeability is 10^{-11} to 10^{-10} m^2. These simulations illustrate how sensitive these systems are to selection of appropriate properties and boundary and initial conditions.

Copyright 2006 by the American Geophysical Union

Components: 17,870 words, 26 figures, 2 tables, 1 dataset.

Keywords: basement outcrop; heat flow; heat flux; hydrothermal circulation; Juan de Fuca Ridge flank; numerical model.

Index Terms: 3015 Marine Geology and Geophysics: Heat flow (benthic); 3017 Marine Geology and Geophysics: Hydrothermal systems (0450, 1034, 3616, 4832, 8135, 8424); 3021 Marine Geology and Geophysics: Marine hydrogeology.

Received 9 January 2006; **Revised** 31 March 2006; **Accepted** 24 April 2006; **Published** 12 July 2006.

Hutnak, M., A. T. Fisher, L. Zühlsdorff, V. Spiess, P. H. Stauffer, and C. W. Gable (2006), Hydrothermal recharge and discharge guided by basement outcrops on 0.7–3.6 Ma seafloor east of the Juan de Fuca Ridge: Observations and numerical models, *Geochem. Geophys. Geosyst.*, *7*, Q07O02, doi:10.1029/2006GC001242.

Theme: Formation and Evolution of Oceanic Crust Formed at Fast Spreading Rates
Guest Editors: Damon A. H. Teagle and Doug Wilson

1. Introduction

[2] Seamounts and other oceanic basement outcrops have long been recognized as important entry and exit points for ridge-flank hydrothermal circulation [e.g., *Jacobson*, 1992; *Johnson et al.*, 1993; *Langseth et al.*, 1984; *Mottl and Wheat*, 1994; *Williams et al.*, 1979], but several recent studies suggest that these features may actually control patterns and rates of fluid circulation in the crust [*Fisher et al.*, 2003a, 2003b; *Harris et al.*, 2004; *Villinger et al.*, 2002]. Widely distributed areas of basement exposure allow hydrothermal fluids to bypass thick layers of low-permeability sediments that cover most of the ocean floor [*Spinelli et al.*, 2004a], helping to explain a global heat flow anomaly (measurements commonly falling below predictions of conductive lithospheric cooling models) that extends on average to seafloor aged $\leq$65 Ma [*Anderson and Hobart*, 1976; *Parsons and Sclater*, 1977; *Stein and Stein*, 1992]. The interpretation that the distribution of areas of basement exposure are a primary control on advective heat loss from the oceanic lithosphere also helps to explain why hydrothermal circulation continues to great age in many areas [*Von Herzen*, 2004]; the fundamental limit is not on hydrothermal convection in the crust per se, but is on the ability of convection to move heat advectively from the crust to the ocean.

[3] Despite the global importance of basement outcrops in removing heat from oceanic lithosphere, relatively little is known about how this process operates, and how observations of basement relief, sediment thickness, and seafloor heat flux might be used to infer rates and patterns of fluid circulation through and near outcrops. To address this deficiency, we synthesize earlier work and present new data collected on the eastern flank of the Juan de Fuca Ridge, one of the best-studied ridge-flank hydrothermal regions on Earth. We present observations of seafloor topography, surface heat flux, and basement structure around individual basement outcrops and use these data to infer the roles of basement outcrops in guiding hydrothermal circulation. We develop conductive and coupled (fluid-heat flow) numerical models of individual basement outcrops and outcrop pairs to estimate crustal properties, driving forces, and fluid temperatures and fluxes. These coupled models allow us to estimate sets of properties and flow conditions that are most consistent with field observations, and illustrate aspects of these systems that remain unconstrained, hopefully to be resolved by future surveys and modeling.

2. Geologic Setting and Previous Work

[4] The Endeavour segment of the Juan de Fuca Ridge (JFR) generates lithosphere west of North America, and contains numerous features common to most ridge flanks: extrusive igneous basement overlain by sediments, abyssal hill topography, high-angle faulting, and basement outcrops (Figures 1 and 2) [e.g., *Davis and Currie*, 1993; *Davis and Lister*, 1977; *Kappel and Ryan*, 1986; *Karsten et al.*, 1986; *Lister*, 1970]. Turbidites flowed onto this region from the continental margin to the east during the Pleistocene, resulting in the accumulation of thick sediments that bury oceanic basement rocks in this area at an unusually young age [*Davis et al.*, 1992; *Underwood et al.*, 2005]. Igneous basement is exposed close to the ridge where the crust is young, and where tectonic and magmatic activity have produced basement relief greater than local sediment thickness.

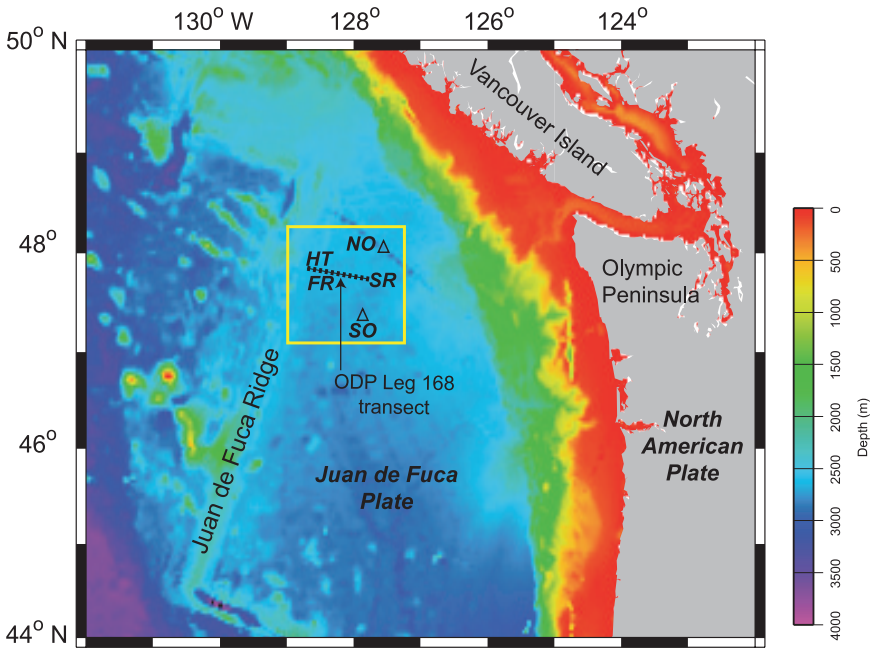

Figure 1. Regional bathymetric map of the northeastern Pacific Ocean (bathymetric data from *Smith and Sandwell* [1997]). ODP Leg 168 drilling transect extends 20–100 km east of the Endeavour segment of the JFR on 0.9 to 3.6 Ma seafloor. IODP Expedition 301 worked on the eastern end of this transect. Yellow box indicates region shown in greater detail in Figure 2. FR, First Ridge area; HT, Hydrothermal Transition area; SR, Second Ridge area; SO, Southern Outcrop area; NO, Northern Outcrop area.

[5] Several earlier studies summarized regional geology, geophysics, and geochemistry on the eastern flank of the JFR [e.g., *Davis et al.*, 1992; *Davis and Currie*, 1993; *Rosenberger et al.*, 2000; *Wheat and Mottl*, 1994; *Zühlsdorff et al.*, 2005], and others have explored specific hydrogeologic settings in this region [e.g., *Becker et al.*, 2000; *Davis et al.*, 1989; *Mottl et al.*, 1998; *Wheat et al.*, 2000]. Ocean Drilling Program (ODP) Leg 168 completed a drilling transect of eight sites across 0.9 to 3.6 Ma seafloor on the eastern flank of the JFR, collecting sediment, rock, and fluid samples; determining thermal, geochemical, and hydrogeologic conditions in basement; and installing a series of long-term borehole observatories in the upper crust [e.g., *Becker and Fisher*, 2000; *Davis et al.*, 1997b, 1999; *Elderfield et al.*, 1999; *Fisher et al.*, 1997, 2000; *Marescotti et al.*, 2000]. Integrated Ocean Drilling Program (IODP) Expedition 301 returned to the eastern end of the ODP Leg 168 transect (Figure 2), known as the Second Ridge (SR) area, to drill deeper into basement; sample additional sediment, basalt, and microbiological materials; and establish a new generation of multilevel observatories as part of a long-term, three-dimensional hydrogeologic experiment [*Fisher et al.*, 2005b].

[6] Much previous work in this region focused on understanding where and how hydrothermal fluids discharge, recharge, or flow laterally through basement. Fluids are thought to recharge the upper crust at the western end of the ODP Leg 168 transect, in the Hydrothermal Transition (HT) area (Figure 2), where seafloor heat flux is low and basement fluids have a chemistry much like bottom seawater [*Davis et al.*, 1992; *Shipboard Scientific Party*, 1997b; *Zühlsdorff et al.*, 2005]. The First Ridge (FR) area is characterized by thin sediment cover over a buried basement high that strikes subparallel to the spreading center to the west, from which highly altered hydrothermal fluids seep at rates up to several centimeters per year [*Giambalvo et al.*, 2000; *Shipboard Scientific Party*, 1997a; *Spinelli et al.*, 2004b; *Wheat and Mottl*, 1994]. At the opposite end of the Leg 168 drilling transect, in the SR area, basement relief is significantly greater and basaltic rocks are exposed through the Papa Bare, Mama Bare, and Baby Bare outcrops [*Becker et al.*, 2000; *Davis et al.*, 1992; *Mottl et al.*, 1998; *Thomson et al.*, 1995].

[7] Baby Bare outcrop is the most extensively surveyed and smallest of the three SR outcrops, rising 70 m above the surrounding seafloor and covering an area of 0.5 km^2 (Table 1). Analysis of

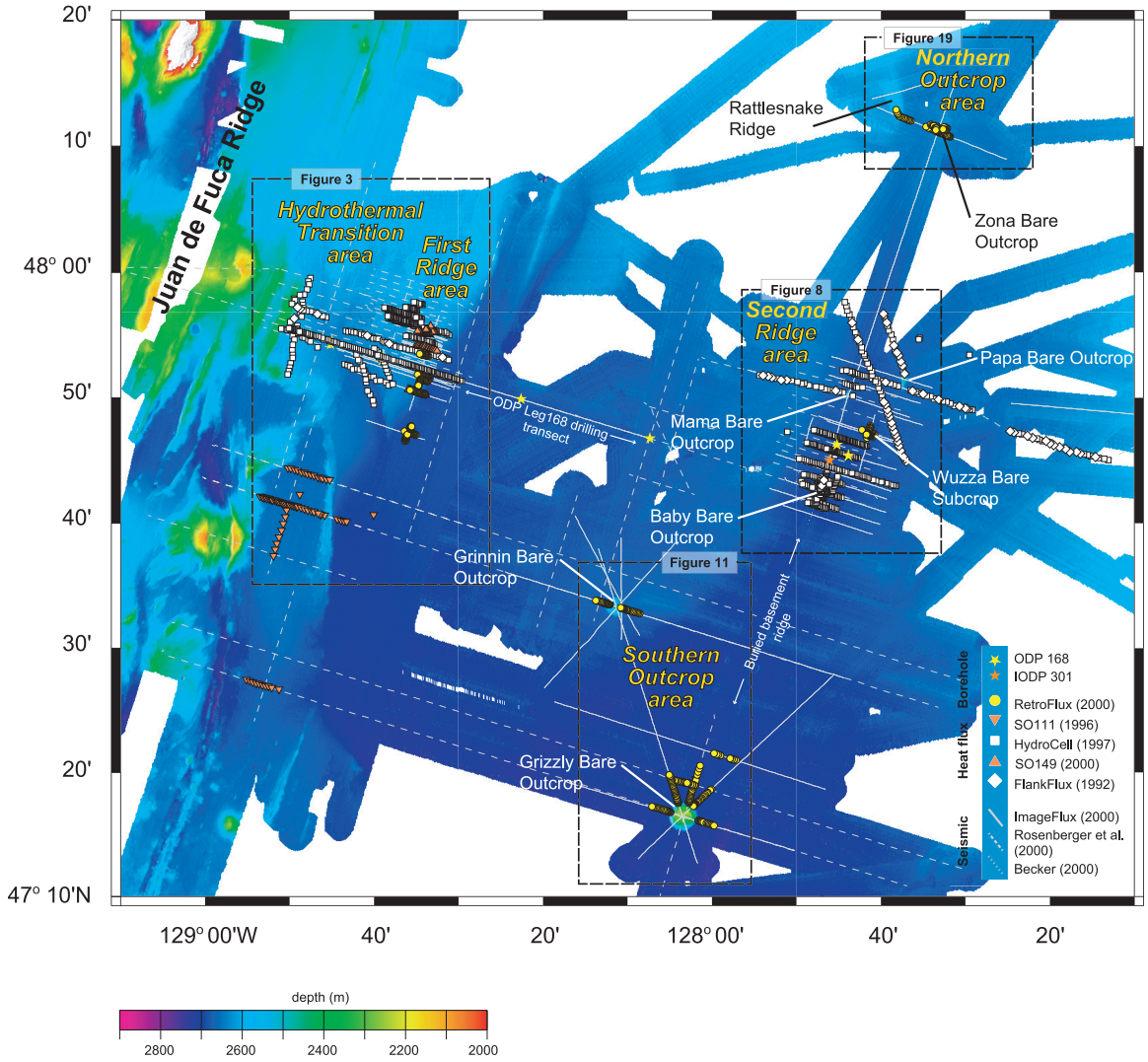

Figure 2. Map of the eastern flank of the JFR using composite swath bathymetry. Seismic track lines from *Davis et al.* [1992], *Rosenberger et al.* [2000], *Becker et al.* [2000], and *Zühlsdorff et al.* [2005], omitting dense coverage over the First Ridge and Second Ridge areas. Heat flux positions from earlier studies by *Davis et al.* [1992] and *Davis et al.* [1997a] are shown as diamonds and squares, respectively, and those from new studies by *Zühlsdorff et al.* [2005] are displayed as circles and triangles. Primary work areas and prominent outcrops and subcrops are shown, as are labeled boxes of local (more detailed) maps.

altered rocks, sediment pore fluids, and shallow thermal gradients on Baby Bare outcrop demonstrate that this feature produces 5–20 L/s of hydrothermal fluid discharge and releases 2–3 MW of heat [*Becker et al.*, 2000; *Mottl et al.*, 1998; *Thomson et al.*, 1995; *Wheat et al.*, 2004]. Fluids seeping from the top of Baby Bare outcrop have an exit temperature near 25°C, but their chemistry indicates alteration at 60–65°C, consistent with nearby borehole measurements and regional estimates of upper basement temperatures.

[8] Survey coverage of Baby Bare outcrop is extensive, and although there is evidence of discharge, no sites of hydrothermal recharge have been observed [*Becker et al.*, 2000; *Wheat et al.*, 2004]. Consideration of ridge-flank hydrothermal driving forces, basement fluid chemistry, and sediment properties preclude recharge of Baby Bare outcrop through the seafloor surrounding the basement edifice; instead, fluids are thought to recharge through Grizzly Bare outcrop 52 km to the south (Figure 2), then transit north to Baby Bare outcrop where they are discharged [*Fisher et al.*, 2003a; *Wheat et al.*, 2000].

Table 1. Basement Outcrops and Survey Areas Discussed

Basement Outcrop Name[a]	Survey Area[a]	Maximum Height Above Surrounding Seafloor, m	Area,[b] km^2
Papa Bare	SR	240	2.6
Mama Bare	SR	140	0.9
Baby Bare	SR	70	0.5
Grizzly Bare	SO	450	9.6
Grinnin' Bare	SO	250	4.9
Zona Bare	NO	70	0.8
N1	HT/FR	100	9.8
N2	HT/FR	100	9.6
N3	HT/FR	100	>20

[a] Outcrop locations and survey areas are shown in Figures 1–3, 8, 11, and 19. SR, Second Ridge area; SO, Southern Outcrop area; NO, Northern Outcrop area; HT, Hydrothermal Transition area; FR, First Ridge area.
[b] Areas are approximate, based on swath map bathymetry and seismic data.

[9] The hydrothermal regimes of Mama and Papa Bare outcrops are less well understood, but both features are primarily thought to be sites of hydrothermal discharge. Mama Bare outcrop is located 14 km northeast of Baby Bare outcrop on the same basement ridge, covers an area of 0.9 km^2, and rises 140 m above the surrounding seafloor. Papa Bare outcrop is built on an adjacent buried basement ridge to the east, covers an area of 2.6 km^2, and rises 240 m above the surrounding seafloor.

3. Recent Surveys and Data Analyses

3.1. Data Acquisition and Processing

[10] Two recent field surveys added considerably to swath-map, seismic, and heat flux coverage of the eastern flank of the JFR: the RetroFlux expedition (R/V *Thomas G. Thompson*, TN116) and the ImageFlux expedition (R/V *Sonne*, SO149). The ImageFlux expedition collected mainly swath-map and seismic data, with limited heat flux surveys, whereas the RetroFlux expedition collected mainly heat flux data and sediment cores, with limited swath-map coverage. An overview of bathymetric, seismic, and heat flux data acquisition and processing is presented by *Zühlsdorff et al.* [2005], with an emphasis on implications for scientific drilling and related experiments; results presented in the present paper focus on outcrops. A compilation of all available heat flux data from this study region, including locations and estimates of measurement uncertainty, is available as a digital supplement[1] to this paper.

3.2. Estimation of Basement Thermal Conditions

[11] We use seismic, heat flux, and drilling data in conjunction with analytical and numerical calculations to estimate thermal conditions in basement. The approach is described in greater detail elsewhere [*Davis et al.*, 1999; *Fisher et al.*, 2005a; *Zühlsdorff et al.*, 2005], and is summarized briefly here. Sediment thicknesses and basement relief were estimated from seismic data using local travel time-to-depth conversions based on drilling results [*Davis et al.*, 1997b, 1999]. Interpreted seafloor and basement horizons were digitized with spatial resolution of <20 m, including an assessment of uncertainties in the location of the sediment-basement interface (SBI). Uncertainties tend to be greatest where the SBI dips steeply and where strongly three-dimensional structures (e.g., some buried or exposed basement highs) are projected onto a two-dimensional seismic profile.

[12] Thermal conditions in upper basement along co-located seismic and heat flux transects were estimated using two methods. First, we extrapolated heat flux data into upper basement by one-dimensional boot-strapping, assuming that heat transport in the sediment column is primarily conductive and vertical [e.g., *Davis et al.*, 1999]. This last assumption is consistent with dominantly conductive conditions in sediment across the field area, based on >1700 multipenetration (shallow) heat flux measurements [*Zühlsdorff et al.*, 2005] and thermal studies in the Leg 168 sediment boreholes [*Pribnow et al.*, 2000]. Only *Alvin*-probe measurements on Baby Bare outcrop, not analyzed in the present paper, have given indications of fluid seepage of sufficient magnitude to perturb conductive thermal gradients [*Wheat et al.*, 2004]. Temperature contours and estimated SBI temperatures shown later in this paper were calculated by boot-strapping, with uncertainty bars on the SBI temperatures being based on combined uncertainties in heat flux values, sediment thermal conductivity, sediment velocity structure, and the location of the SBI in seismic profiles.

[13] We also generated two-dimensional simulations of conductive heat flux along the seismic profiles using a numerical model [*Zyvoloski et al.*, 1996]. This approach differs from one-dimensional boot-strapping in that it allows for conductive thermal refraction resulting from basement relief

[1] Auxiliary material is available at ftp://ftp.agu.org/apend/gc/2006gc001242.

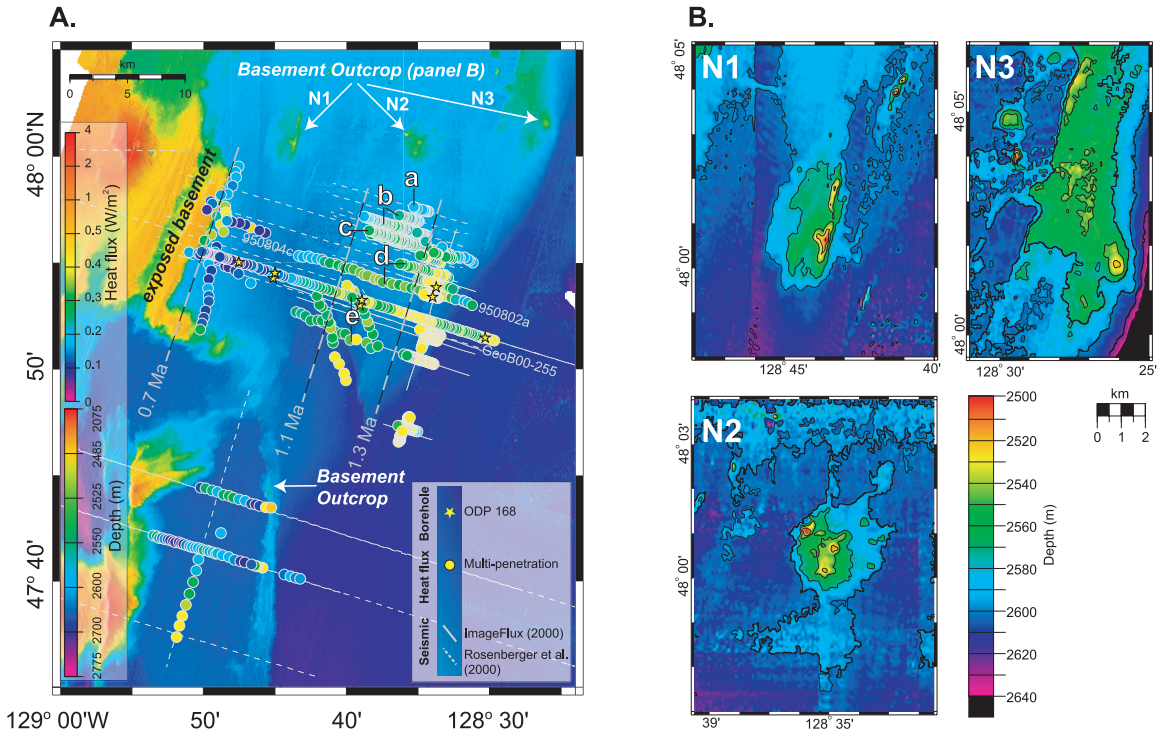

Figure 3. (a) Map of the Hydrothermal Transition (HT) and First Ridge (FR) areas, with co-located seismic track lines and heat flux values overlain on swath bathymetry. Map location shown in Figure 2. Approximate basement ages based on magnetic anomalies [*Currie et al.*, 1982]. Extremely dense seismic coverage over First Ridge area is not shown [*Zühlsdorff et al.*, 2005]. Labeled seismic lines (950804c/950802a and GeoB00-255) are shown in Figures 4 and 5. Note locations of previously unpublished basement outcrops on the northern edge of the HT and FR areas (N1, N2, N3; displayed in Figure 3b), and additional areas of basement exposure to the south. Possible implications of these outcrops for fluid circulation are discussed in the text, based on gathering of heat flux data into statistically distinct groups labeled a, b, c, d, and e (Figure 7). (b) Detailed bathymetry of basement outcrops N1, N2, and N3. Contour interval is 25 m.

and contrasts in sediment and basement thermal properties, and allows generation of continuous calculated heat flux and SBI temperature profiles. Finite element grids were created for each seismic profile for which there were co-located heat flux data, with grid geometry based on 50–100 m subsamples of digitized seafloor and basement horizons, sediment and basement properties based on drilling and lab results [e.g., *Giambalvo et al.*, 2000; *Shipboard Scientific Party*, 1997d; *Spinelli et al.*, 2004a], and an upper (seafloor) boundary held at a constant bottom water temperature of 2°C. For modeled profiles across the HT and FR region, the basal boundary condition (set several kilometers below the top of basement), was heat flux estimated using a standard lithospheric cooling curve [*Parsons and Sclater*, 1977]. The thermal boundary condition set at the base of models of the SR, SO, and NO areas was set at 180 mW/m^2, based on observations away from the perturbing influence of buried or exposed basement highs [*Zühlsdorff et al.*, 2005].

4. Survey Results and Analytical Calculations

4.1. Hydrothermal Transition (HT) and First Ridge (FR) Areas

[14] Bathymetric data from the HT and FR areas reveal several notable features (Figure 3a), including a broad region of exposed basement at the western end of the Leg168 drilling transect, a linear basement outcrop striking subparallel to the primary tectonic fabric south of the HT area, and three prominent basement outcrops north and northeast of the HT and FR areas. The lack of seismic reflection profiles across these three outcrops precludes a definitive assessment of the amount of exposed basement, but the high slope angles between the outcrops and surrounding turbidite plain

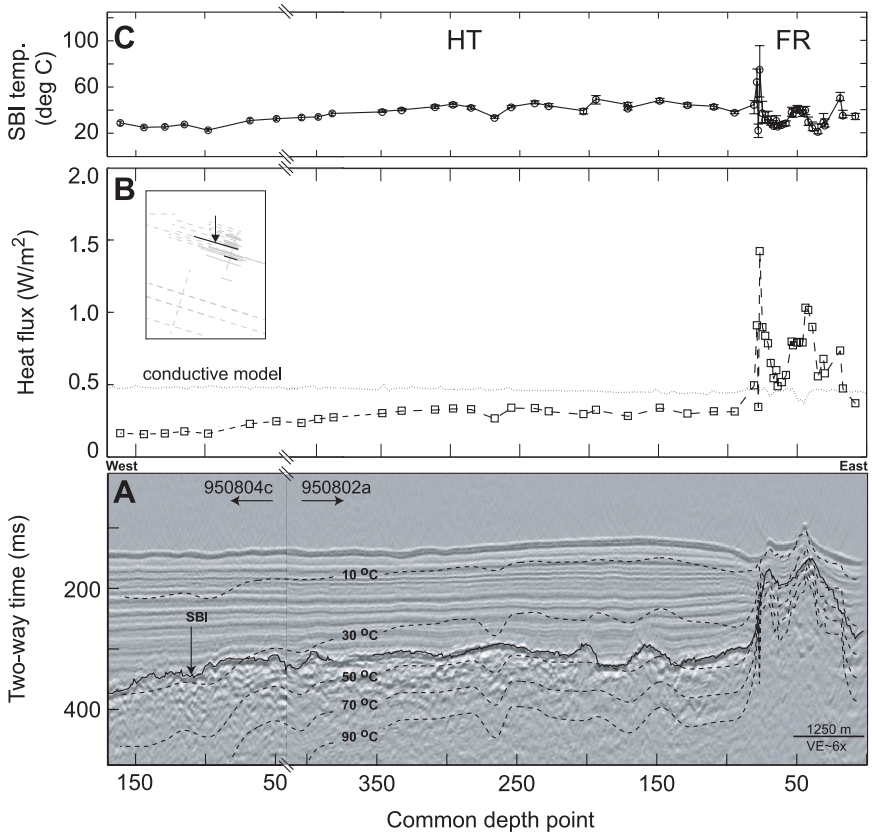

Figure 4. Seismic data, heat flux data, and calculated sediment/basement interface (SBI) temperatures along a composite of seismic Lines 950804c and 950802a (locations in Figure 3). Analytical and numerical methods described in the text. (a) Seismic data with superimposed isotherms calculated from seafloor heat flux data. Seismic acquisition and processing described by *Rosenberger et al.* [2000]. VE, vertical exaggeration. (b) Heat flux data (open squares connected by dashed line) and calculated from a two-dimensional conductive model, based on conductive lithospheric cooling (dotted line). Uncertainties in measurements are smaller than symbols. Inset shows regional seismic tracklines (gray) in relation to transects presented in the current manuscript (black). Arrow indicates transect in the current figure. (c) Estimated SBI temperatures based on one-dimensional boot-strapping of field data (circles and solid connecting line), with uncertainties indicated by vertical bars. FR, First Ridge area; HT, Hydrothermal Transition area.

are incapable of supporting a significant sediment cover (Figure 3b and Table 1).

[15] Outcrop N1 is elongate and strikes to the northeast, roughly 12 km NNE of the ODP Leg 168 drilling transect. It is 2.5 km wide, 5 km long, rises roughly 100 m above the surrounding seafloor, and covers and area of 9.8 km^2 (Table 1). Much of the feature appears relatively flat, but there are two prominent high points along the eastern edge where the seafloor relief is greatest. Outcrop N2 is more conical in shape and also rises roughly 100 m above the surrounding seafloor. This feature has a diameter of 3–4 km and is topped with three individual peaks. The highest slope angles are found on the northwestern peak, where seafloor elevation changes by roughly 110 m over a lateral distance of 200 m. Outcrop N3 consists of an elongate bathymetric high striking to the northeast, and also has several prominent local peaks where igneous basement is likely exposed. The entire feature covers an area of >20 km^2, and rises roughly 100 m above the turbidite plain at its highest point.

[16] As described in several earlier studies, there is a systematic increase in heat flux with distance from the area of broad basement exposure at the western edge of the HT area [*Davis et al.*, 1992, 1997a, 1999]. Heat flux rises from ~15% of lithospheric conductive values close to the point of sediment onlap, to ~100% of lithospheric values (with significant local variability) over the buried basement high in the FR area, as shown along seismic lines 950804c and 950802a (Figure 4).

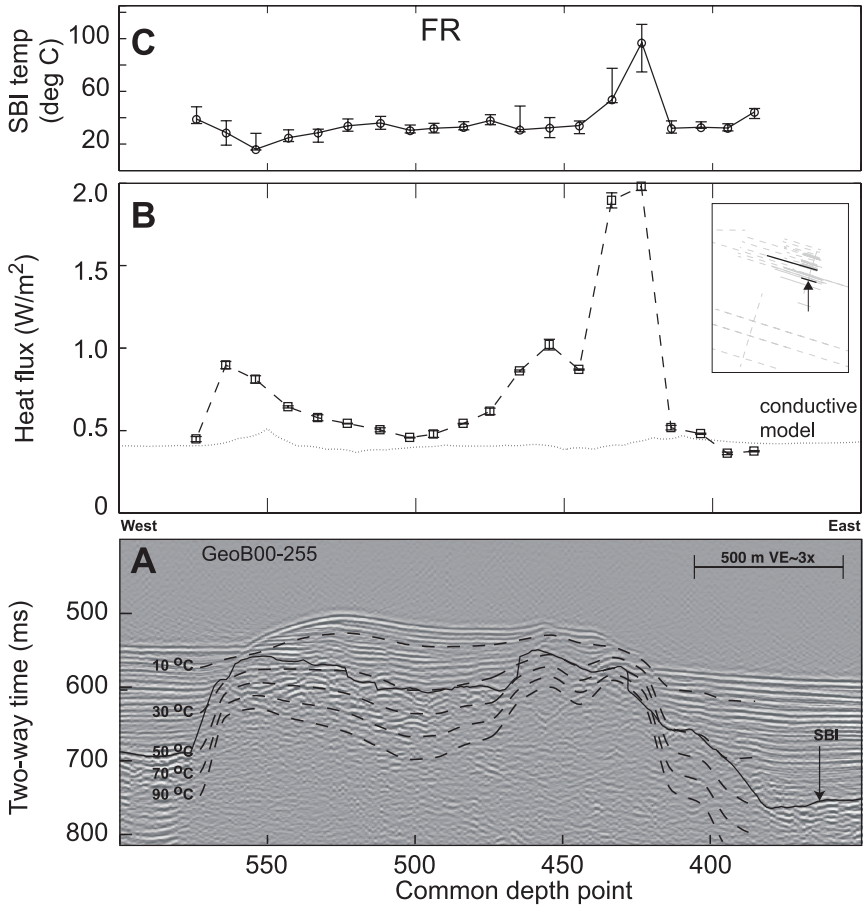

Figure 5. Seismic and heat flux data and calculated SBI temperatures along seismic line GeoB00-255 in the FR area (location shown in Figure 3). Symbols and nomenclature as in Figure 4. (a) Seismic data. Seismic acquisition and processing described by *Zühlsdorff et al.* [2005]. (b) Heat flux and conductive model calculations. (c) Estimated SBI temperatures. Results are characteristic of thermal homogenization of upper basement along the buried basement ridge.

Calculated SBI temperatures increase commensurately from 20°C in the central HT area to 40°C west of the FR area, although sediment thickness remains roughly constant and basal heat flux predicted with lithospheric cooling curves decreases significantly. Basement temperatures along this transect remain relatively constant across the FR buried basement high, despite variations in basement elevation of ~125 m, illustrating relative isothermality thought to be induced by local vigorous convection. The SBI across the FR basement high is particularly well imaged along seismic line GeoB00-225, 3 km to the south (Figure 5). There is a single seafloor high, but seismic data reveal two local basement peaks at depth. Seafloor heat flux is elevated above both basement peaks (nearly 1 W/m^2 on the western peak and 2 W/m^2 on the eastern peak), but SBI temperatures are relatively consistent.

[17] The broad pattern of heat flux suppression across the HT area is consistent with extraction of lithospheric heat by fluids that enter the crust to the west, where there is a large area of exposed basement close to the active spreading center, and flow to the east at rates of meters to tens of meters per year [e.g., *Davis et al.*, 1997b, 1999; *Elderfield et al.*, 1999; *Stein and Fisher*, 2003]. However, it is difficult to explain how fluid entering from the west can flow rapidly to the east without there being a region of exposed basement through which these fluids can reenter the ocean. The driving forces for ridge-flank hydrothermal circulation in this area are modest, on the order of tens of kilopascals, and sediment permeabilities are much too low to allow thermally significant fluid seepage, even where sediment thickness is only a few tens of meters [e.g., *Giambalvo et al.*, 2000; *Spinelli et al.*, 2004a, 2004b; *Wheat and Mottl*, 1994]. In addition, very young fluid in the FR area relative to fluid in the HT

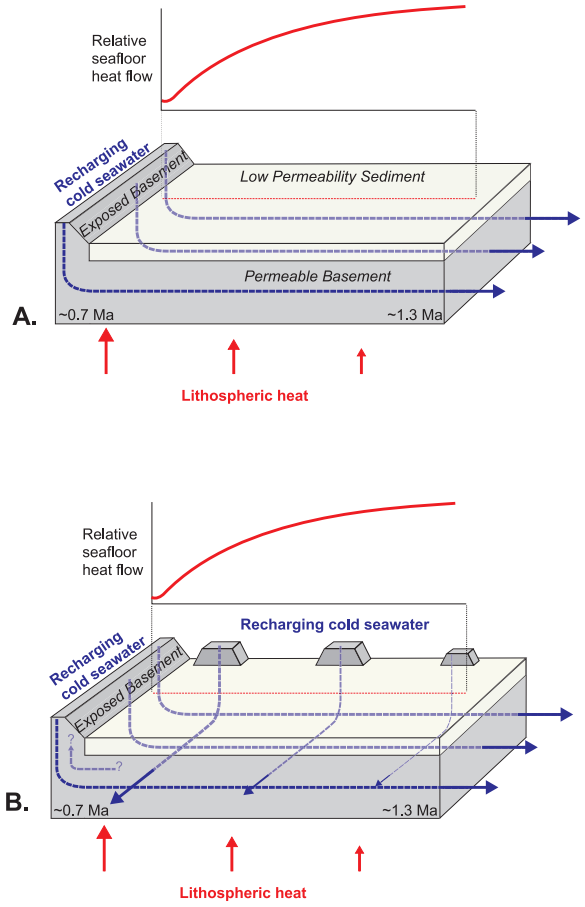

Figure 6. Conceptual models of the geometry of ridge-flank hydrothermal circulation across the Hydrothermal Transition (HT) area. (a) Cold seawater recharges exposed basement rocks to the west of the HT area and flows rapidly to the east [*Davis et al.*, 1992; *Elderfield et al.*, 1999; *Shipboard Scientific Party*, 1997c]. This flow geometry could lead to the observed pattern of seafloor heat flux, with very low values to the west and higher values to the east, but suffers from the lack of potential discharge points east of the HT area [e.g., *Davis et al.*, 1999]. (b) Newly identified basement outcrops (Figure 3) may allow fluid recharge north of the HT area, with discharge occurring to the south (or possibly to the west). This model is tested through examination of north-to-south variations in seafloor heat flux across the HT area. Actual fluid flow patterns in basement in this area are likely to be more complex than either of these idealized cartoons suggest.

area to the west, as indicated by ^{14}C ages of upper basement pore waters [*Elderfield et al.*, 1999], cannot be explained by recharge from the west and dominant flow to the east.

[18] One explanation for both thermal and ^{14}C observations is a significant component of north-to-south fluid flow in basement across the HT and FR areas, perhaps in combination with a west-to-east component (Figure 6). The large number of high-quality heat flux data across the HT area, particularly on seafloor aged 1.1 to 1.3 Ma, allow this hypothesis to be tested. We created five data groups from available HT transects using two nonparametric statistical tests. The Mann-Whitney test ranks data based on their magnitude [*Siegel*, 1956], whereas the Kolomogorov-Smirnov test is based on probability-density functions of data sets [*Press et al.*, 1989]. Both tests provide a quantitative assessment as to whether subsets of data are likely to comprise parts of a larger data set, or whether they are better considered to be distinct data sets. We used both methods to determine whether individual heat flux transects across the HT area on 1.1 to 1.3 Ma seafloor could be considered to comprise distinct data sets at the 95% confidence level.

[19] There is little or no trend when the grouped data are plotted against crustal age, but there is a strong trend when the data are plotted against linear distance from the nearest outcrop north of the HT area (N2; Figures 3 and 7). Sediment thickness is relatively constant within the swath of seafloor represented by these thermal data; the spatial trend in seafloor heat flux is not a result of sediment thinning to the south above isothermal basement. Instead, both seafloor heat flux and upper basement temperatures rise from north to south. These data are compared to calculations based on a one-dimensional, well-mixed aquifer model [*Langseth and Herman*, 1981; *Rosenberg et al.*, 2000] to evaluate what volumetric fluid fluxes (volume flow rate/cross-sectional area) in the upper crust may be implied by the data (Figure 7b). On the basis of a typical sediment thickness above basement in this area of 200 m, and assuming that crustal fluids flow mainly in an upper basement aquifer 300 m thick, a fluid flux of ~1 m/yr is inferred. The average particle velocity of fluid in basement depends on the effective porosity of the aquifer, but is likely to be at least 10–20 times greater. Variations in aquifer thickness, aquifer depth, sediment thickness, and other parameters would result in commensurately different calculated fluxes. A fluid flux of 1 m/yr is at the low end of those estimated in earlier studies that assumed a dominantly west-to-east flow direction [*Davis et al.*, 1999; *Elderfield et al.*, 1999; *Stein and Fisher*, 2001b].

[20] Actual fluid flow patterns in basement in this area are likely to be more complex than suggested by these simple models, including mixed convec-

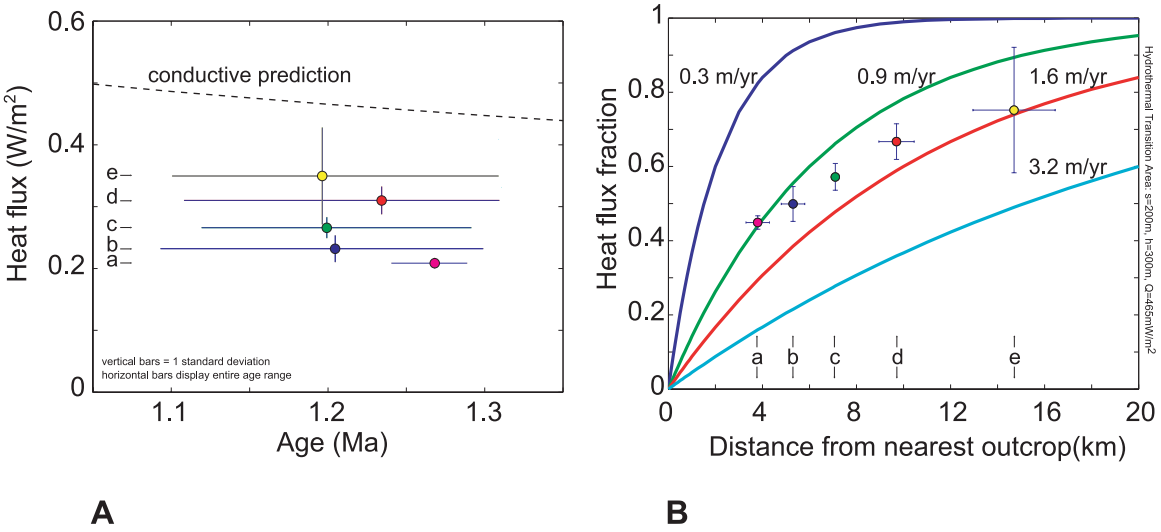

Figure 7. Evaluation of the possibility of north-to-south fluid flow across the HT area based on the distribution of data on 1.1 to 1.3 Ma seafloor. Data from heat flux transects were grouped using nonparametric statistical tests to evaluate how to combine them, with final groupings shown in Figure 3. (a) Heat flux data group means plotted versus crustal age, showing little or no consistent trend. Vertical bars show one standard deviation of each group, whereas the horizontal bars show the range of seafloor ages. (b) Group means plotted against distance from the nearest outcrop, with heat flux values converted to heat flux fraction (observed value/conductive lithospheric value, based on crustal age). There is a strong correlation between heat flux and distance from the nearest outcrop. Solid lines show calculations based on the one-dimensional well-mixed aquifer model for rapid lateral fluid flow in basement [*Langseth and Herman*, 1981], as described in the text.

tion helping to homogenize upper basement temperatures locally [e.g., *Davis et al.*, 1999; *Stein and Fisher*, 2003]. North-to-south flow may be favored by structural trends in basement, as inferred in the SR area 60 km to the east [*Fisher et al.*, 2003a; *Wheat et al.*, 2000], with fluid traveling "along strike" within preferential flow paths developed as the crust is constructed and faulted along trends parallel to the active ridge. A modest component of north-to-south flow in the FR area may also help to explain anomalously young ^{14}C ages estimated for fluids recovered during ODP Leg 168 drilling [*Elderfield et al.*, 1999].

4.2. Second Ridge (SR) Area

[21] Swath map bathymetric data collected prior to the RetroFlux and ImageFlux expeditions included the three main basement outcrops in the SR area: Baby Bare, Mama Bare and Papa Bare, but additional data collected during recent expeditions help to fill gaps in coverage between the outcrops (Figure 8a). Mutlipenetration heat flux measurements in this area range from 0.03 to 4 W/m^2, with the highest values found adjacent to outcrops that are known sites of hydrothermal discharge and/or situated directly above shallowly buried basement highs [e.g., *Becker et al.*, 2000; *Davis et al.*, 1989, 1992; *Zühlsdorff et al.*, 2005].

[22] Heat flux above the buried basement high between Baby and Mama Bare outcrops is elevated relative to adjacent areas where basement is deeper, with a subtle increase in heat flow from south to north (Figure 8a). This heat flux pattern is associated with basement shoaling in an area where upper basement temperatures are nearly isothermal, and contrasts with that seen in the HT area where heat flow decreases significantly to the north but basement depth remains relatively constant (Figures 3 and 7).

[23] When data from 3.4–3.6 Ma seafloor over and near buried basement highs are excluded (from the SR, SO, and NO areas: Figure 2), removing both anomalously high and low values, the heat flux through the surrounding seafloor averages 181 ± 16 mW/m^2 [*Zühlsdorff et al.*, 2005], significantly lower than values of 251–272 mW/m^2 predicted by lithospheric cooling models [*Lister*, 1977; *Parsons and Sclater*, 1977; *Stein and Stein*, 1992]. Even after correcting for the effects of sedimentation (as much as 15–16% [*Davis et al.*, 1999]), the observed seafloor heat flux is low relative to conductive predictions by 15–20%. This result differs from that presented by *Davis et*

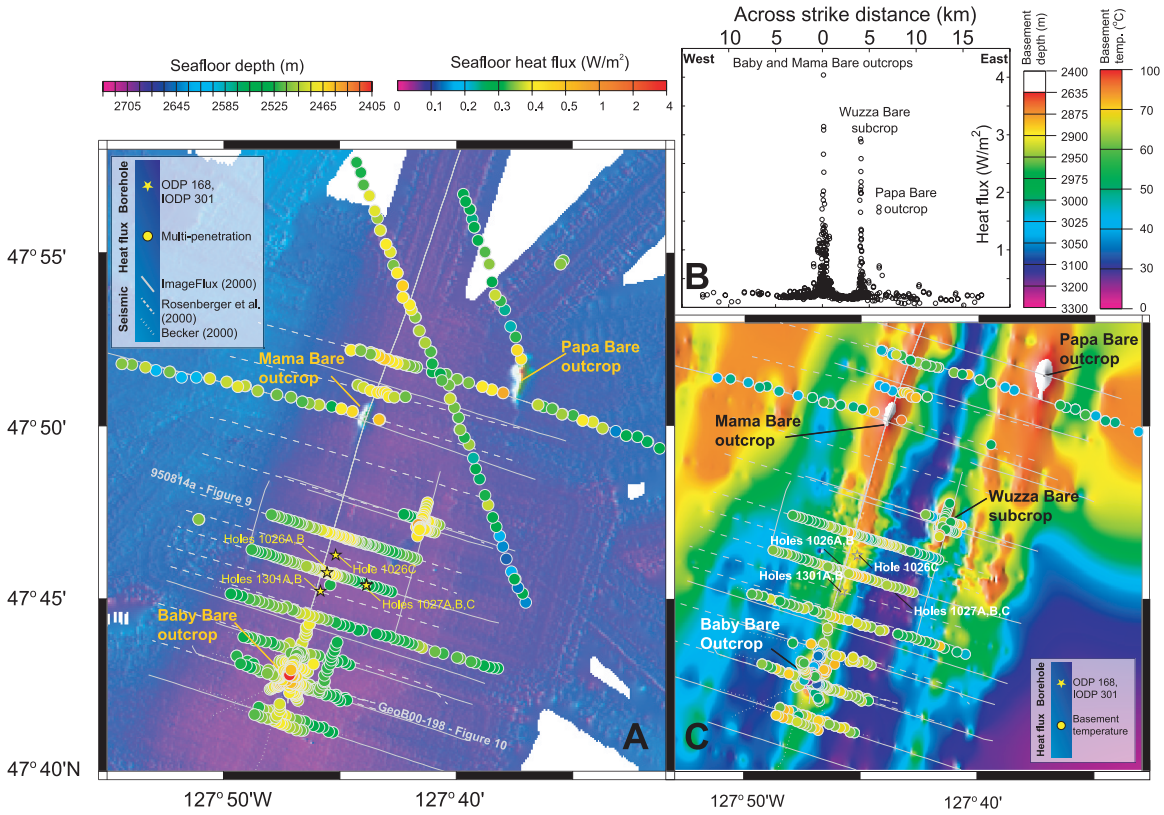

Figure 8. Bathymetry, heat flux, basement relief, and calculated temperatures at the sediment-basement interface (SBI) in the Second Ridge (SR) area. (a) Bathymetry and heat flux. Labeled seismic and heat flux transects are shown in later figures. Note consistently higher heat flux across buried basement ridge that strikes north-northeast, along the trend of Baby Bare to Mama Bare outcrops. (b) Heat flux from the SR area plotted along a west-east transect originating at the buried basement high, illustrating extreme consistency in a direction along structural strike and strong cross-strike variability. Locations of individual basement highs are labeled. Wuzza Bare subcrop is a shallowly buried basement high that generates a strong local heat flux high and from which highly altered basement fluids seep [*Zühlsdorff et al.*, 2005]. (c) Basement relief calculated from regional bathymetry and dozens of seismic lines across the SR area [*Zühlsdorff et al.*, 2005], with SBI temperatures shown where there are high-quality, co-located seismic and heat flux data. SBI temperatures are not estimated immediately above local basement highs because of large uncertainties in sediment thickness and difficulties in downward continuing one-dimensional heat flux values. Note relative consistency of upper basement temperatures across the SR area above and adjacent to the buried basement ridge.

al. [1999] because that study examined a single transect crossing ODP Sites 1026 and 1027, whereas the present study includes an analysis of heat flux within a swath of 3.4–3.6 Ma seafloor extending 100 km from north to south. The low conductive heat flux could result from regionally lower lithospheric heat flux compared to global averages, large-scale advective heat loss from the crust (equally affecting a 100-km-long swath of seafloor extending from the NO area to the SO area, Figure 2), or bias in the distribution of heat flux measurements [*Zühlsdorff et al.*, 2005], with more measurements made close to basement outcrops. None of these explanations is entirely satisfying, and hopefully the conundrum can be resolved through limited future measurements on 3.4–3.6 Ma seafloor in this region that are far from outcrops or buried basement highs.

[24] Co-located seismic and heat flux profiles across the SR basement high illustrate two characteristic relationships. Where basement is completely buried by sediments, heat flux is generally greatest just above the basement peak (365 mW/m^2 along seismic line 950814a north of ODP Site 1026; Figure 9). Heat flux approaches 180 mW/m^2 on either side of the buried basement high, and upper basement temperatures remain relatively uniform

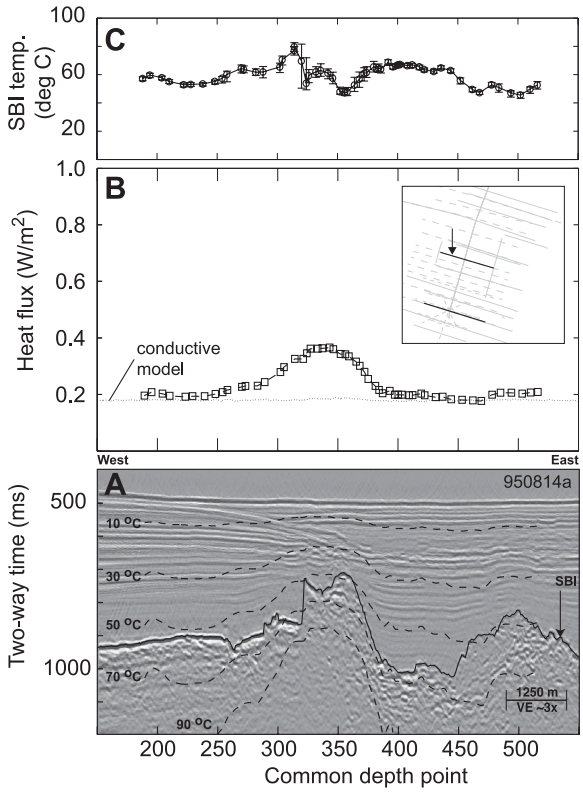

Figure 9. Seismic, heat flux, and calculated sediment/basement interface (SBI) temperatures along seismic line 950814a north of Baby Bare outcrop across the SR area (location shown in Figure 8a). Symbols and nomenclature as in Figure 4. (a) Seismic data and calculated isotherms. Seismic acquisition and processing discussed by *Rosenberger et al.* [2000]. (b) Heat flux data and conductive model calculations. (c) Estimated SBI temperatures. Results are characteristic of thermal homogenization of upper basement across the SR area.

near 60°C. Upper basement temperatures are remarkably uniform along the buried basement high from Baby Bare outcrop to north of Mama Bare outcrop, a distance of 16 km [e.g., *Davis et al.*, 1992, 1997b; *Fisher et al.*, 2005a] (Figure 8b).

[25] Heat flux data co-located along seismic line GeoB00-198 crossing Baby Bare outcrop display a pattern characteristic of fluid and heat transport toward, and discharge from, an exposed basement outcrop (Figure 10). Heat flux is relatively uniform around 170–190 mW/m^2 at lateral distances >1.5 km from the limit of basement exposure, and rise monotonically to >800 mW/m^2 near the edge of the outcrop. Conductive thermal refraction can account for only 50–75 mW/m^2 of the observed increase in heat flux, and this begins only 50–100 m from the outcrop edge. The remaining elevation in heat flux near the outcrop edge results from the flow of warm fluid that rises from depth, sweeping isotherms upward in shallow basement [*Fisher et al.*, 2003a] (Figure 10a). Later in this paper we show numerical models of this process that replicate the near-outcrop heat flux profiles.

4.3. Southern Outcrop (SO) Area

[26] Bathymetric data from the SO area show two basement outcrops rising above the otherwise flat and thickly sedimented seafloor (Figures 2 and 11). Grizzly Bare outcrop is located 52 km south-southwest of Baby Bare outcrop, along the same direction as the abyssal hill upon which Baby Bare and Mama Bare outcrops are located. This outcrop is conical in shape, 3.5 km in diameter, and rises 450 m above the surrounding seafloor (Table 1).

[27] The tectonic and volcanic relationships between the SR outcrops and Grizzly Bare outcrop are unclear. The consistency of their alignment and strike with regional basement topography [*Shipboard Scientific Party*, 1997c; *Wilson*, 1993; *Zühlsdorff et al.*, 2005] suggests that the Grizzly, Baby, and Mama Bare outcrops could be located on the same buried abyssal hill. Thermal and chemical data suggest that there is fluid flow in basement between Grizzly Bare and Baby Bare outcrops, perhaps in part because of enhanced basement permeability in the along-strike direction [*Fisher et al.*, 2003a; *Wheat et al.*, 2000]. However, seismic lines between Grizzly Bare and Baby Bare outcrops show that the buried basement high below Baby Bare and Mama Bare outcrops is largely absent to the south, reappearing immediately north of Grizzly Bare outcrop. Also, regional marine magnetic anomalies [*Wilson*, 1993] suggest that Grizzly Bare outcrop may be located on crust that is 100–200 k.y. younger than that below Baby and Mama Bare outcrops. The age of Grizzly Bare outcrop is unknown, but Baby Bare outcrop is thought to have formed from an off-axis eruption, being as much as 800 k.y. younger than the crust on which it sits [*Becker et al.*, 2000; *Karsten et al.*, 1998].

[28] Grinnin' Bare outcrop, located 33 km north-northwest of Grizzly Bare outcrop, appears to have been conical in form originally, but roughly 1/3 of its exposed mass has collapsed along a steeply dipping failure surface on its eastern side (Figure 11b). The exposed edifice rises 250 above the surrounding seafloor, and was 2.5–3.0 km in diameter prior to the collapse. Although both Grinnin' and Grizzly Bare outcrops were known

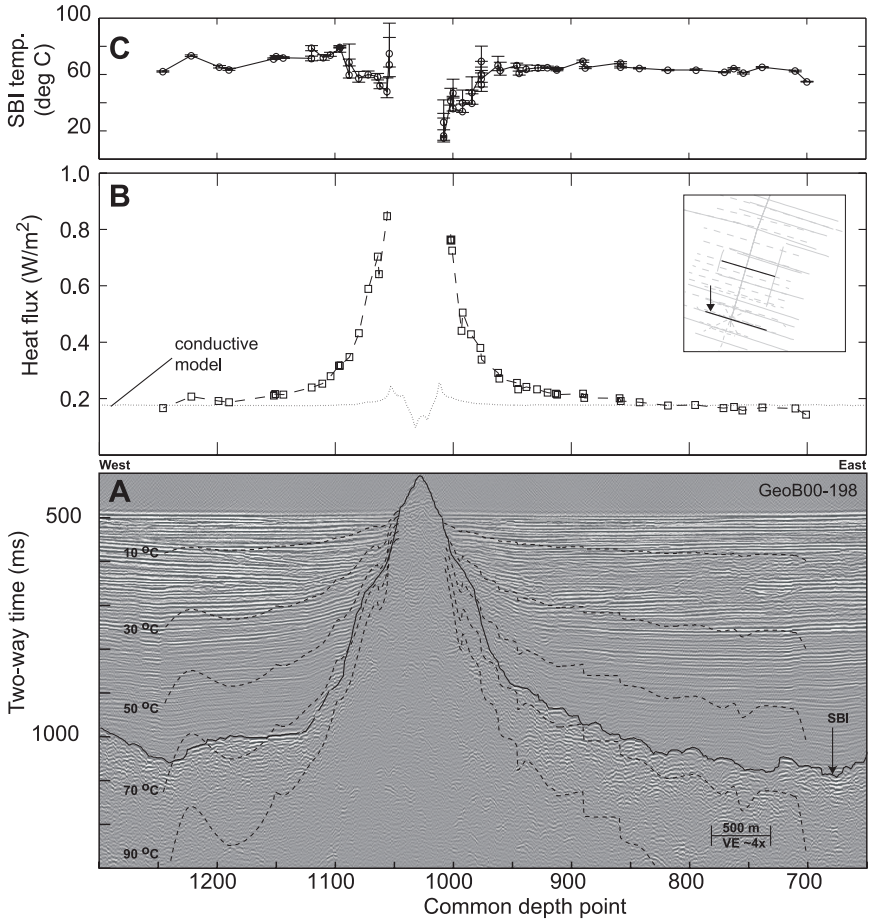

Figure 10. Seismic, heat flux, and calculated sediment/basement interface (SBI) temperatures along seismic line GeoB00-198 across Baby Bare outcrop (location shown in Figures 8a and 8c; data from *Fisher et al.* [2003a]). Symbols and nomenclature as in Figure 4. (a) Seismic data and calculated isotherms. Seismic acquisition and processing discussed by *Zühlsdorff et al.* [2005]. (b) Heat flux data and conductive model calculations. (c) Estimated SBI temperatures. Note background heat flux values far from the outcrop around 180 mW/m^2 and upper basement temperatures of 60–65°C. Calculated isotherms at outcrop edge are swept upward by discharging hydrothermal fluids.

to exist prior to the RetroFlux and ImageFlux expeditions, the recent surveys generated continuous swath bathymetric data between these features and the SR area to the north, multiple seismic lines crossing both outcrops, and co-located heat flux data that allow the first assessment of crustal thermal conditions near these features.

[29] Heat flux data were collected along seven transects in the vicinity of Grizzly Bare outcrop, five as profiles extending radially away from the area of exposed basement, and two as ''across-strike'' profiles to the north of the outcrop (Figure 11). Collectively these profiles demonstrate that Grizzly Bare outcrop is a site of ridge-flank hydrothermal recharge, but they also show complexity in fluid and heat flux patterns and the influence of multiple processes. Heat flux values near the outcrop range from 80 to 400 mW/m^2, with the lowest values found close to the outcrop on the eastern and western profiles, and the highest values found close to the outcrop on the northern side.

[30] Heat flux data co-located on east-to-west seismic line GeoB00-176 are the clearest with regard to fluid flow. Heat flux is relatively constant at 175–185 mW/m^2 at distances >1 km from the outcrop, consistent with the local background values seen to the north, but drops abruptly to 80–100 mW/m^2 closer to the outcrop edge (Figure 12). Conductive thermal refraction should result in somewhat greater heat flux immediately adjacent to the outcrop (Figure 12b), so the observed decreases are particularly significant. Estimated temperatures in basement show that isotherms are swept downward near the outcrop edge (Figure 12a),

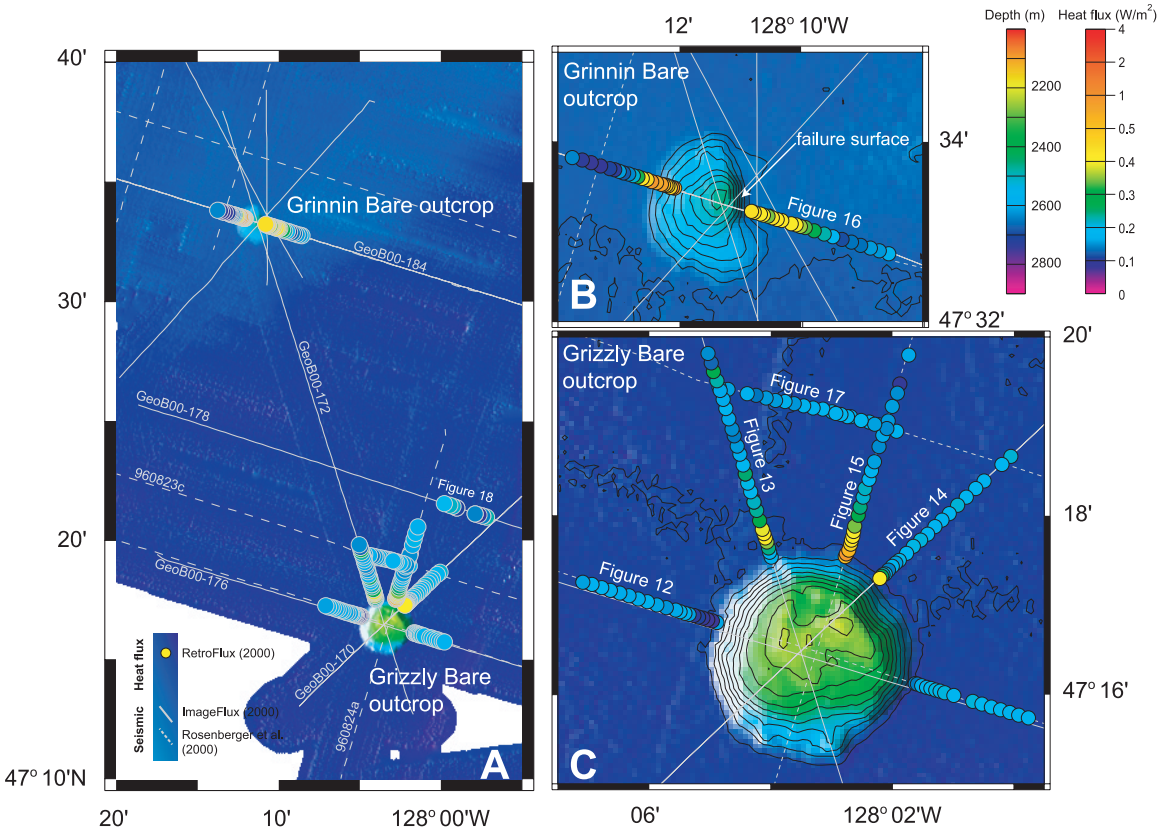

Figure 11. Maps of the Southern Outcrop area. Location shown in Figure 2. Composite swath bathymetry from *Zühlsdorff et al.* [2005]. Seismic track lines from *Rosenberger et al.* [2000] and *Zühlsdorff et al.* [2005]. All heat flux data are from most recent survey. (a) Southern Outcrop area showing Grizzly Bare and Grinnin' Bare outcrops, separated by 33 km. (b) Grinnin' Bare outcrop detail map showing heat flux over bathymetry. Seismic and heat flux profile along line GeoB00-184 shown in Figure 16. (c) Grizzly Bare outcrop detail map showing heat flux over bathymetry. Seismic and heat flux profiles along seismic lines are shown in later figures, as labeled.

a pattern that contrasts sharply with that seen in basement close to Baby Bare outcrop, a site of hydrothermal discharge (Figure 10).

[31] Heat flux data co-located along seismic line GeoB00-172, extending radially to the northwest from Grizzly Bare outcrop (roughly toward Grinnin' Bare outcrop, Figure 11), display a more complex pattern. Heat flux along much of the profile is 180–200 mW/m^2, but rises to >400 mW/m^2 close to the outcrop and drops back to 180 mW/m^2 near the limit of basement exposure (Figure 13). The heat flux high is positioned above a small buried basement platform, suggesting that the thermal signal may result partly from basement relief if basement temperatures are kept locally isothermal by small-scale convection. On a broader scale, basement isotherms appear to be swept downward near the edge of the outcrop (Figure 13a), as seen along line GeoB00-176 (Figure 12).

[32] Heat flux data co-located along seismic line GeoB00-170, extending radially to the northeast from Grizzly Bare outcrop (Figure 11), are also relatively uniform around 180–200 mW/m^2 at distances >500 m from the outcrop edge (Figure 14). Values rise to >400 mW/m^2 near the limit of basement exposure, more than can be explained by conductive refraction (Figure 14b), but isotherms are suppressed adjacent to the edifice (Figure 14a). Heat flux data co-located on seismic line 960824a extending radially north from Grizzly Bare outcrop (Figure 11) rise from 180 mW/m^2 to nearly 1 W/m^2 near the limit of basement exposure (Figure 15). This pattern suggests that there may be an area of fluid discharge along the northern edge of Grizzly Bare outcrop, or perhaps local convection in basement, but the near-edifice isotherms are not swept upward as abruptly as near Baby Bare outcrop (Figures 10a and 15a). As shown later in a series of conductive and coupled radial models, heat flux can rise in the vicinity of a recharging outcrop depend-

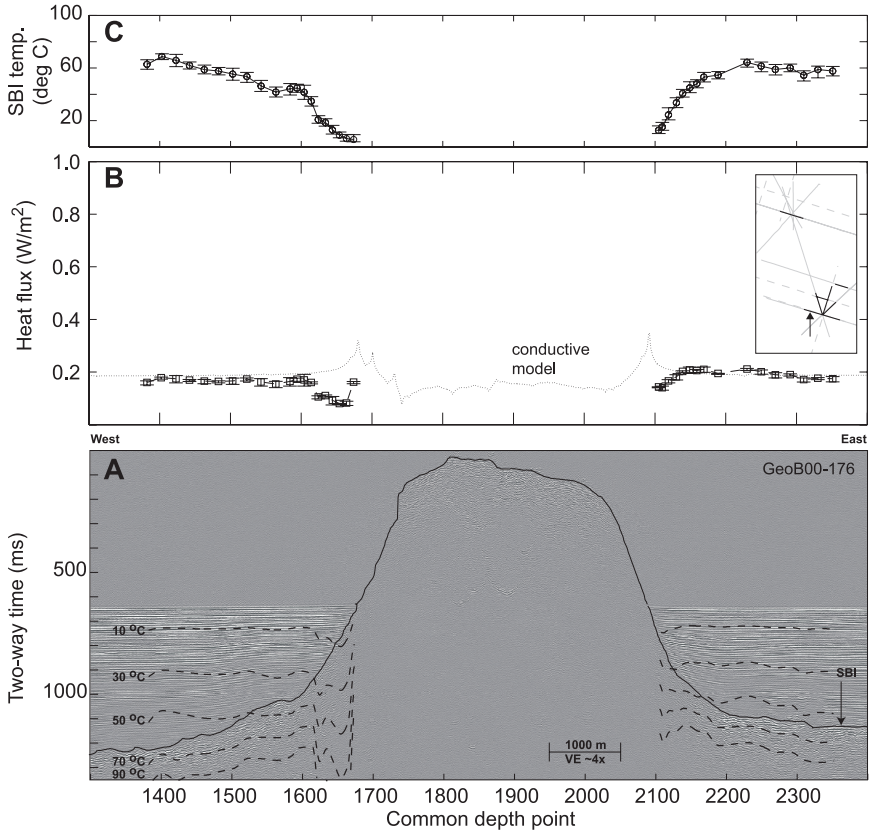

Figure 12. Seismic, heat flux, and calculated sediment/basement interface (SBI) temperatures along seismic line GeoB00-176 across Grizzly Bare outcrop (location shown in Figures 11a and 11c; data from *Fisher et al.* [2003a]). Symbols and nomenclature as in Figure 4. (a) Seismic data and calculated isotherms. Seismic acquisition and processing discussed by *Zühlsdorff et al.* [2005]. (b) Heat flux data and conductive model calculations. (c) Estimated SBI temperatures. Note background heat flux values far from the outcrop around 180 mW/m^2 and upper basement temperatures of 60–65°C. Calculated isotherms at outcrop edge are swept downward by recharging seawater.

ing on flow patterns and rates, particularly in the presence of local convection. Given the size of Grizzly Bare outcrop it is not surprising that hydrogeologic conditions appear to be heterogeneous.

[33] Fewer data are available adjacent to Grinnin' Bare outcrop (Figures 11 and 16). Two heat flux transects were run along seismic line GeoB00-184 to the west and east of the basement edifice. Far from the outcrop, heat flux is typically 170–190 mW/m^2. Heat flux rises to almost 1 W/m^2 near the limit of basement exposure on the western side of the outcrop. This transect was continued up the sloping side of the edifice, where a thin (seismically transparent) veneer of sediment allowed penetration of a short heat flow lance, yielding heat flux values >2 W/m^2 (Figure 16b). The heat flux pattern is more complex on the profile east of the outcrop where the transect crosses the buried slide block that resulted from failure of this side of the edifice, and values immediately adjacent to the outcrop edge exceed 700 mW/m^2. Collectively, these heat flux data are most consistent with the hypothesis that Grinnin' Bare outcrop is a site of hydrothermal discharge, but it is a relatively large feature and data are limited, so we cannot dismiss the possibility of hydrothermal recharge somewhere on the edifice.

[34] Heat flux values co-located along seismic line 960823c, oriented east-west, northwest of Grizzly Bare outcrop and southeast of Grinnin' Bare outcrop (Figures 11 and 17), are remarkably uniform around 180–190 mW/m^2, but there is a buried basement high below the western part of the transect within which basement temperatures are lower than seen elsewhere in this area. Typical upper basement temperatures are 60–65°C in this region, but values along the buried basement high are only 40–50°C. One explanation is that heat flux is entirely conductive and these upper basement temperatures result from basement being

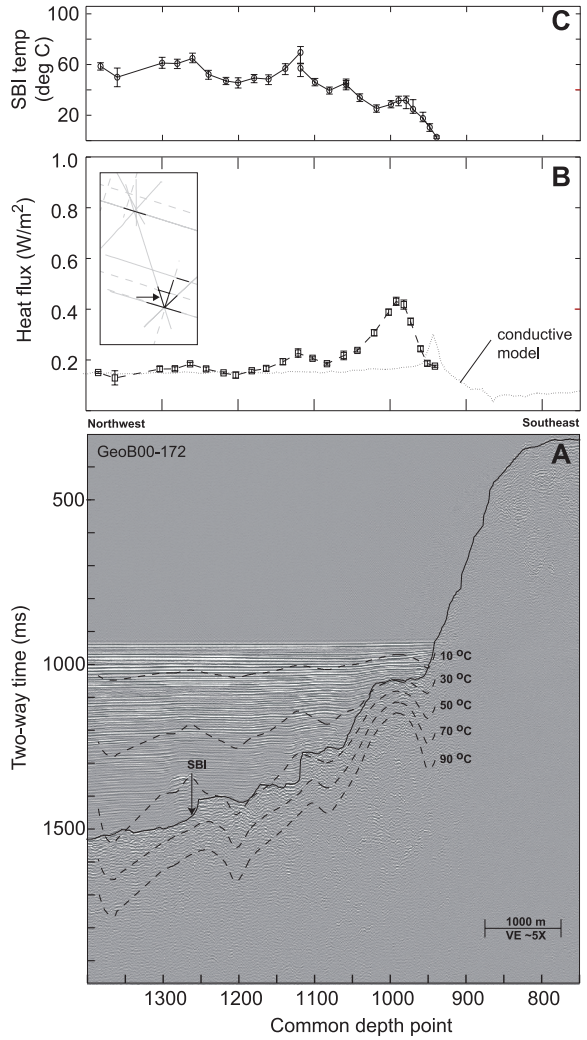

Figure 13. Seismic, heat flux, and calculated sediment/basement interface (SBI) temperatures along seismic line GeoB00-172 northwest from Grizzly Bare outcrop (location shown in Figures 11a and 11c). Symbols and nomenclature as in Figure 4. (a) Seismic data and calculated isotherms. Seismic acquisition and processing discussed in *Zühlsdorff et al.* [2005]. (b) Heat flux data and conductive model calculations. (c) Estimated SBI temperatures. Calculated isotherms at outcrop edge are swept downward by recharging seawater, whereas the local heat flux high may be associated with secondary convection in basement, as discussed in text.

shallower, but there could also be modest temperature suppression resulting from cold fluid recharge through Grizzly Bare outcrop to the south (Figures 17a and 17b).

[35] The heat flux distribution along seismic line GeoB00-178, oriented east-west to the northeast of Grizzly Bare outcrop is more provocative (Figure 18). The buried basement high upon which Grizzly Bare outcrop is located is readily apparent in the seismic line, although it tapers out farther to the north, and heat fluxes immediately above the eastern side of the basement high are 100 mW/m^2 lower than those to the west. This pattern contrasts sharply with that seen above the buried basement high in the SR area (Figure 9). Local convection in the latter area leads to near-isothermality in upper basement, resulting in seafloor heat flux being higher above the basement high. Lower heat flux above the buried basement high north of Grizzly Bare outcrop requires suppression of basement temperatures by 30–40°C relative to those seen in basement regionally (Figure 18c). These heat flux data were part of a much longer and more detailed transect of measurements, many of which were unsuccessful because the probe continued to sink in the sandy sediments after penetration. The data shown are from very high quality measurements, but they are sparse in distribution.

[36] One possible explanation for the heat flux and basement temperature patterns seen along both seismic lines 960823c and GeoB00-178 (Figures 17 and 18) is that they result from the flow of cool fluid in basement that recharged through Grizzly Bare outcrop to the south. There are prospective sites of hydrothermal discharge north of both of these profiles: Baby Bare outcrop northeast of line 960823c and Grinnin' Bare outcrop northwest of line GeoB00-178. Unfortunately, the heat flux data are limited and the variations along seismic line 960823c are subtle, so additional thermal surveys will be needed to test this hypothesis.

4.4. Northern Outcrop (NO) Area

[37] The RetroFlux and ImageFlux expeditions also explored thermal and hydrogeologic conditions on and near two basement highs located 50 km north-northeast of the SR area, as distant as the SO area is to the south (Figure 2). A basement outcrop had been identified in the NO area while collecting swath map data during a *Sonne* transit in 1996, but bathymetric coverage was limited and there were no seismic data across this area until the more recent surveys [*Zühlsdorff et al.*, 2005]. Two bathymetric highs have been identified in the NO area: Rattlesnake Ridge and Zona Bare outcrop (Figure 19).

[38] Rattlesnake Ridge is an elongate bathymetric high striking toward to the northwest. The seafloor here is as much as 100 m shallower than the surrounding area, but the ridge slopes gently

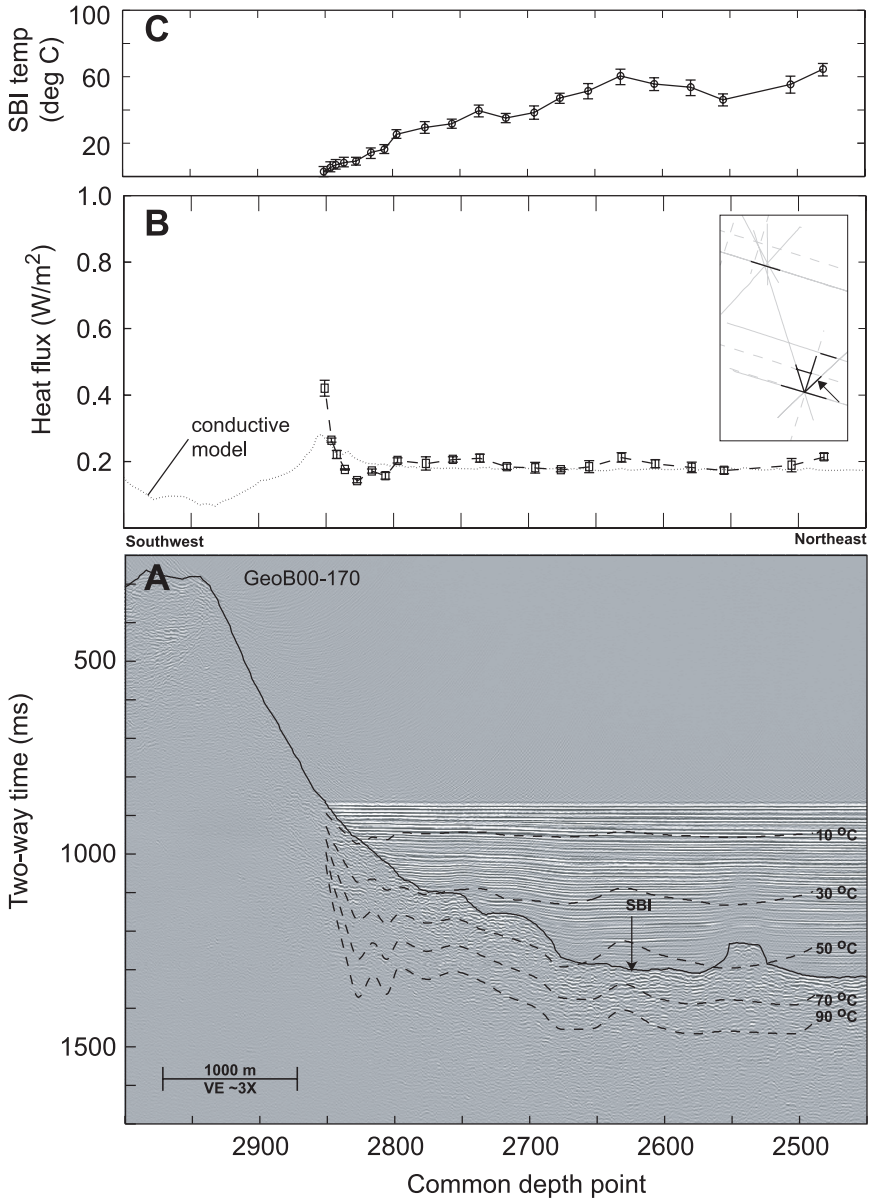

Figure 14. Seismic, heat flux, and calculated sediment/basement interface (SBI) temperatures along seismic line GeoB00-170 northeast from Grizzly Bare outcrop (location shown in Figures 11a and 11c). Symbols and nomenclature as in Figure 4. (a) Seismic data and calculated isotherms. Seismic acquisition and processing discussed by *Zühlsdorff et al.* [2005]. (b) Heat flux data and conductive model calculations. (c) Estimated SBI temperatures. Calculated isotherms at outcrop edge may be slightly depressed, but conditions appear to be largely conductive.

downward on all sides; basement does not appear to be exposed. Seafloor heat flux is 180–210 mW/m^2 approaching and above Rattlesnake Ridge, and unlike the SR region to the south, thermal conditions below the ridge appear to be dominantly conductive (Figures 19 and 20).

[39] In contrast, there is good evidence for hydrogeologic activity within Zona Bare outcrop (Figures 19 and 20). Zona Bare outcrop is elongate and strikes to the northeast. It is 2 km long, 1 km wide, and rises 70 m above the surrounding seafloor (Table 1). The southwestern edge of the outcrop is steeper than the other sides, whereas the top is virtually flat. Heat flux west of Zona Bare outcrop is typically 160–200 mW/m^2, but rises abruptly to >700 mW/m^2 above a buried basement ridge south of the outcrop, and is elevated east of the outcrop as well (Figures 19 and 20b). Basement

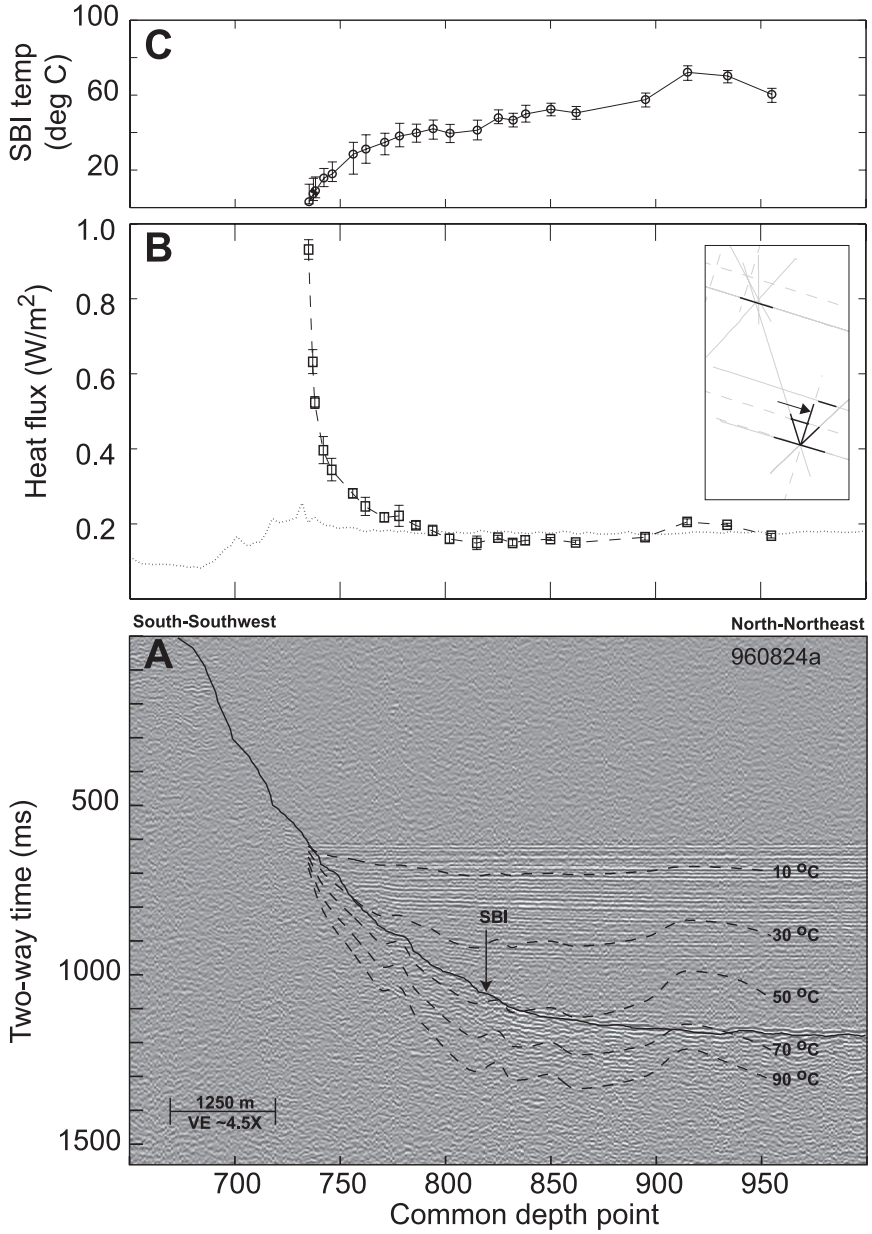

Figure 15. Seismic, heat flux, and calculated sediment/basement interface (SBI) temperatures along seismic line 960824a north of Grizzly Bare outcrop (location shown in Figures 11a and 11c). Symbols and nomenclature as in Figure 4. (a) Seismic data and calculated isotherms. Seismic acquisition and processing discussed by *Rosenberger et al.* [2000]. (b) Heat flux data and conductive model calculations. (c) Estimated SBI temperatures. Unlike other profiles adjacent to Grizzly Bare outcrop, this one may indicate discharge of basement fluid; the abrupt rise in heat flux at the outcrop edge is greater than can be explained by conductive refraction. However, fluid convection in permeable basement can generate a similar thermal effect without requiring discharge (Figures 24d and 24e). Given the size of Grizzly Bare outcrop, it is not surprising that the fluid flow pattern associated with this feature may be heterogeneous.

isotherms appear to follow basement relief, as in the SR and SO areas to the south, suggesting that local convection helps to maintain relatively isothermal conditions in the upper crust. Most of the heat flux data collected adjacent to Zona Bare outcrop are not co-located with seismic profiles, making quantitative interpretation of outcrop thermal and hydrogeologic conditions difficult, but the pattern of heat flux measurements is generally consistent

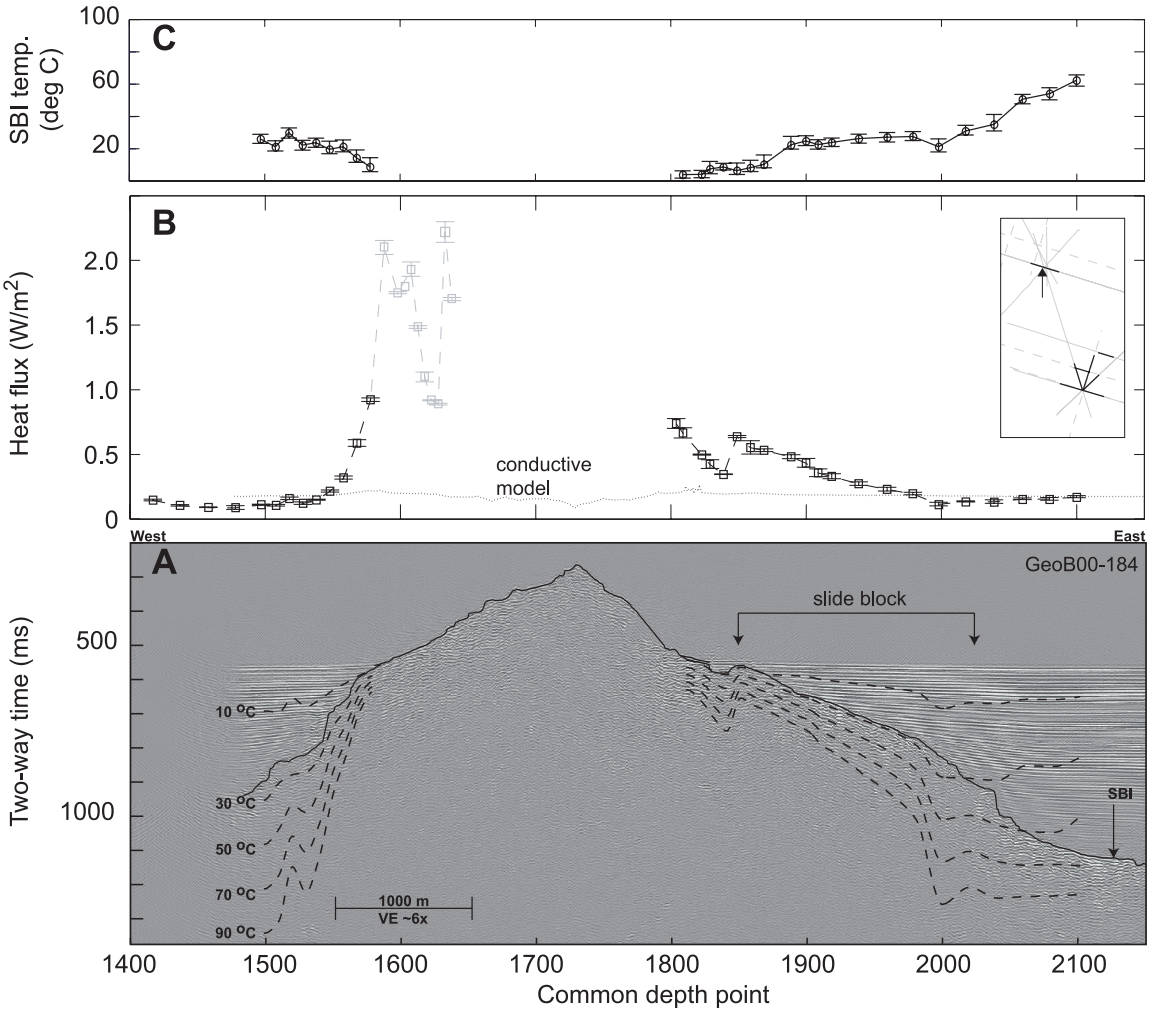

Figure 16. Seismic, heat flux, and calculated sediment/basement interface (SBI) temperatures along seismic line GeoB00-184 across Grinnin' Bare outcrop (location shown in Figures 11a and 11b). Symbols and nomenclature as in Figure 4. (a) Seismic data and calculated isotherms. Seismic acquisition and processing discussed by *Zühlsdorff et al.* [2005]. (b) Heat flux data and conductive model calculations. Gray symbols represent values on the edifice where sediment thickness could not be determined seismically. (c) Estimated SBI temperatures. Note background heat flux values far from the outcrop around 180 mW/m^2 and upper basement temperatures approach 60°C to the east of the outcrop. Calculated isotherms at outcrop edge appear to be swept upward, particularly on the western side. Thermal conditions are more complex on the eastern side of the outcrop, at least in part because of a large slide block shallowly buried below sediments near the edge of the edifice.

with Zona Bare outcrop being another site of ridge-flank hydrothermal discharge.

[40] Several sediment cores targeting the slope-break on the western side of the Zona Bare edifice were collected during the RetroFlux expedition, recovering highly altered pore fluids and clam shells from the top of one weight stand (after it tipped over rather than penetrating the seafloor when it struck the edge of the outcrop). It is not apparent where fluids discharging at Zona Bare outcrop might originate. One possibility is that fluids recharge through Zona Bare itself, perhaps where seafloor heat flux is low along the western edge of the outcrop (Figures 19 and 20), but hydrothermally altered pore fluids were recovered from this area and the broad pattern of heat flux around the outcrop is most suggestive of fluid discharge. Rattlesnake Ridge is not a likely recharge site because there does not appear to be basement exposed on this feature. It is possible that fluids discharging through Zona Bare outcrop recharge through outcrops to the south in the SR or SO areas, or perhaps through nearer, unidenti-

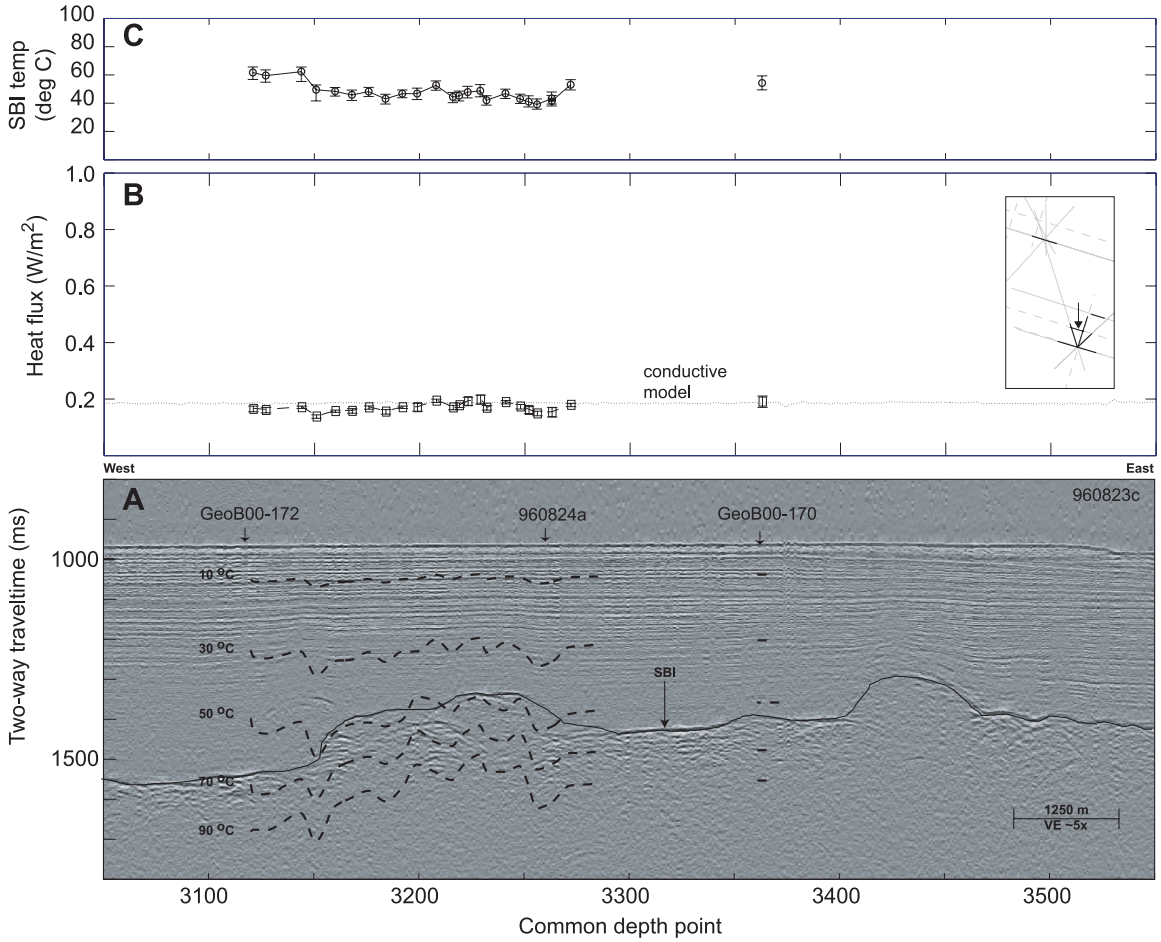

Figure 17. Seismic, heat flux, and calculated sediment/basement interface (SBI) temperatures along seismic line 960823c, between Grizzly Bare and Grinnin' Bare outcrops (location shown in Figures 11a and 11c). Symbols and nomenclature as in Figure 4. (a) Seismic data and calculated isotherms. Seismic acquisition and processing discussed by *Rosenberger et al.* [2000]. (b) Heat flux data and conductive model calculations. (c) Estimated SBI temperatures. Heat flux along this transect is remarkably uniform, despite significant basement relief, leading to upper basement temperatures above a local basement high being 10–20°C cooler than in basement throughout much of the SO, SR, and NO areas. Conditions here appear to be largely conductive or might result from modest thermal suppression as a result of cool fluid recharge through Grizzly Bare outcrop to the south.

fied outcrops in regions lacking high-resolution bathymetric data. Future surveys may help to resolve this question.

5. Numerical Modeling of Hydrothermal Circulation Guided by Outcrops

5.1. Model Design and Constraints

[41] The survey data shown in the previous sections illustrate several settings where there is focused hydrothermal recharge or discharge through basement outcrops. In this section, we show results from two sets of computer models used to evaluate hydrogeologic conditions and processes associated with ridge-flank hydrothermal circulation through basement outcrops.

[42] The first set of models is based on a two-dimensional radially symmetric representation of individual discharging and recharging outcrops. The second set of models is based on a two-dimensional representation of a recharging-discharging outcrop pair separated by 50 km. Properties and processes within and around Baby Bare and Grizzly Bare outcrops were used to design and constrain these simulations (Table 2), which were completed with FEHM, a transient, finite element, heat- and mass transfer code [*Zyvoloski et al.*, 1996]. We have modified FEHM to use a wide

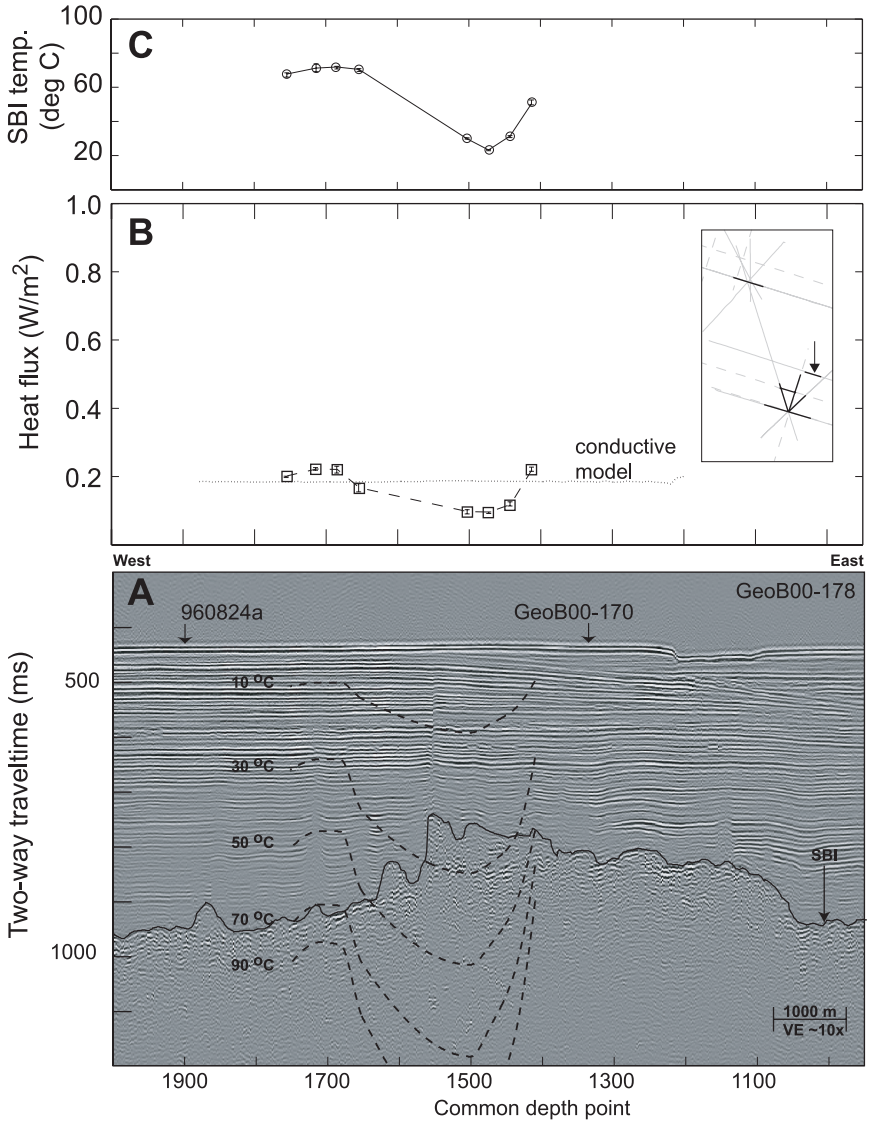

Figure 18. Seismic, heat flux, and calculated sediment/basement interface (SBI) temperatures along seismic line GeoB00-178 north of Grizzly Bare outcrop (location shown in Figure 11a). Symbols and nomenclature as in Figure 4. (a) Seismic data and calculated isotherms. Seismic acquisition and processing discussed by *Zühlsdorff et al.* [2005]. (b) Heat flux data and conductive model calculations. (c) Estimated SBI temperatures. Heat flux values are highly variable along this transect. Several additional measurements were attempted along this profile, but sandy turbidites limited probe penetration in some instances and led to continuous probe sinking in others. The data shown are of high quality, with uncertainties indicated by vertical bars, generally smaller than symbols plotted. Heat flux is lower than conductive predictions by ~50% on the eastern side of the profile, above a buried basement high, suggesting suppression of upper basement temperatures by 30–50°C relative to nearby values of 60–65°C. One explanation is that fluids recharging through Grizzly Bare outcrop to the south flow north within this buried basement high, perhaps eventually venting at Baby Bare outcrop [e.g., *Fisher et al.*, 2003a; *Wheat et al.*, 2000].

range of pressure-temperature conditions appropriate for seafloor hydrothermal systems. FEHM is uses a volume-element formulation and can handle unstructured grids, including layers that pinch out (e.g., sediments around basement outcrops). Model constraints include seafloor heat flux, fluid velocities inferred from pore fluid geochemistry, apparent fluid ages, and pressure differences inferred from sediment and basement data. The primary goals in crafting these models are to gain a quantitative understanding as to factors that may control ridge-flank hydrothermal circulation through seamounts, and how circulation paths and rates may influence seafloor thermal data.

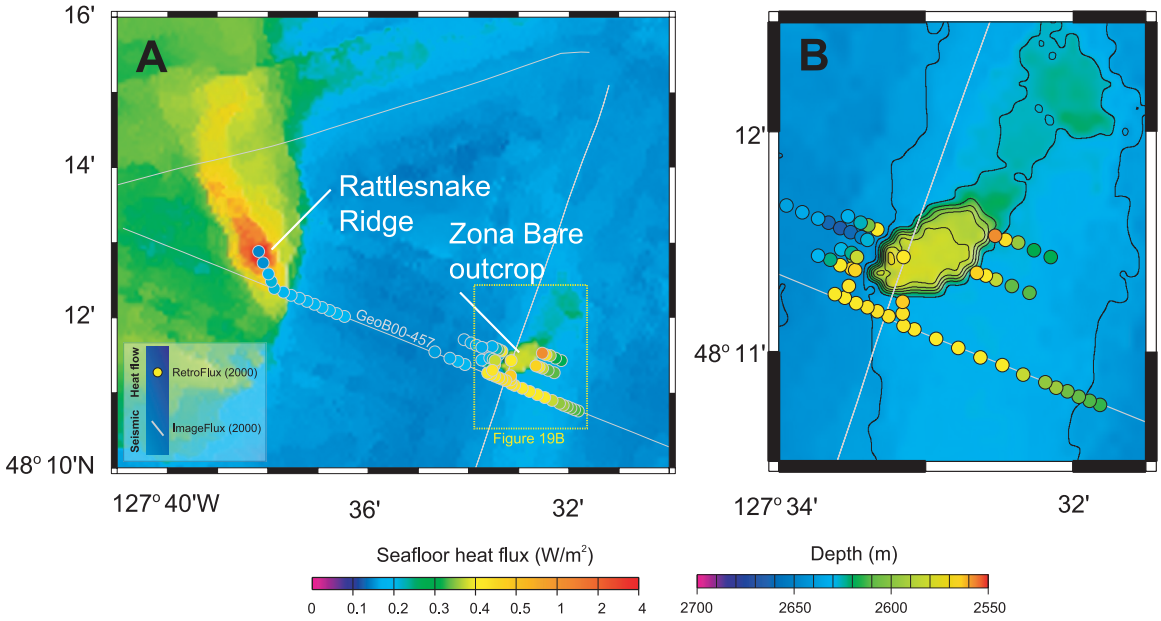

Figure 19. Maps of the Northern Outcrop area. Location shown in Figure 2. Composite swath bathymetry and seismic track lines from *Zühlsdorff et al.* [2005]. Heat flux data are from most recent survey. (a) Northern Outcrop area showing Zona Bare outcrop and Rattlesnake Ridge. Dotted yellow box indicates location of Figure 19b. Data along seismic profile GeoB00-457 shown in Figure 20. Note low heat flux across Rattlesnake Ridge, upon which there is no exposed basement. In contrast, heat flux is highly elevated around much of Zona Bare outcrop. (b) Detail map of Zona Bare outcrop showing distribution of seafloor heat flux. Values are elevated along the southern and eastern side and on the top of this feature but are suppressed within a small area on the western side of the outcrop. Seismic coverage across this feature is unfortunately limited, so thermal and hydrogeologic conditions within basement remain somewhat uncertain.

Models such as these are necessarily idealized, particularly with regard to simplified system geometries and property distributions, but they provide useful insights and help to guide future surveys.

[43] In single-outcrop simulations, the model domain consists of a radial grid 21 km wide (42 km in diameter) and 5 km high (Figure 21). The model domains are tall enough so that lithospheric heat can be input at depth below the crustal aquifer and be redistributed by fluid flow in the shallow crust. Fluid is injected or withdrawn at great distance from the basement outcrops along the "far field" domain boundary. These models include up to six basalt types (having independent properties), overlain by sediments that pinch out at the edge of an exposed basement edifice. The node spacing in these grids is 20–500 m, with finer spacing within the basaltic edifice and coarser spacing in the far field (Figure 21). Because single-outcrop systems are radial, there are no azimuthal variations in processes, only variations in elevation and distance.

[44] One set of single-outcrop models is designed to replicate conditions within and adjacent to Baby Bare outcrop, and another set is intended to replicate conditions within and around Grizzly Bare outcrop. The sides of both edifices slope downward at ~35°, consistent with bathymetric and seismic data. Because there is no reasonable way to simulate free flow in radial coordinates (recharge would occur gradually through an enormous "ring" far from the outcrop, precluding creation of a hydrothermal siphon required to sustain flow [e.g., *Stein and Fisher*, 2003; *Fisher et al.*, 2003a]), all single outcrop simulations are forced-flow models. Fluid is injected or extracted along the far-field model domain at rates consistent with field observations [*Fisher et al.*, 2003a; *Mottl et al.*, 1998; *Thomson et al.*, 1995], then allowed to flow toward or away from the outcrop while convecting freely within the basement aquifer.[*Fisher et al.*, 2003a; *Mottl et al.*, 1998; *Thomson et al.*, 1995]. These simulations are helpful in understanding the thermal seafloor expressions of fluid recharge and discharge near outcrops, and the development of

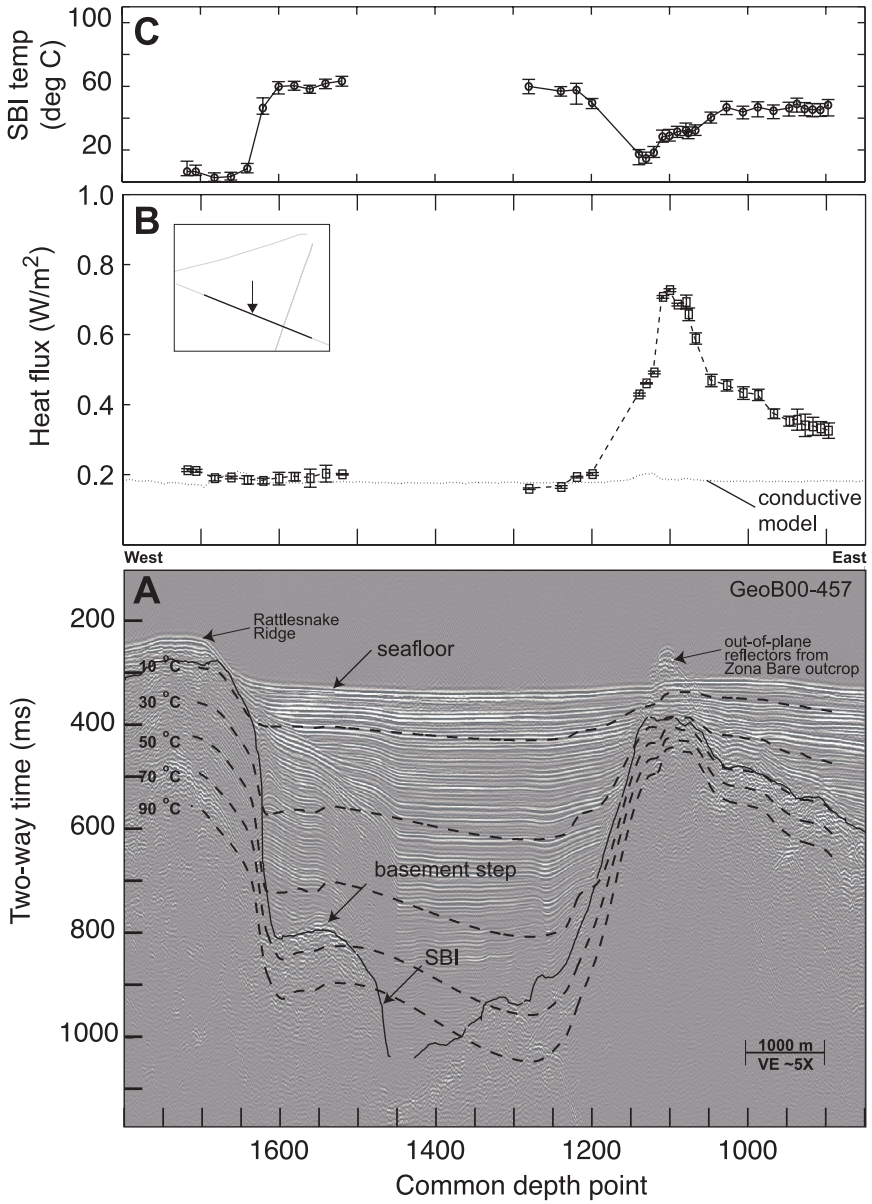

Figure 20. Seismic, heat flux, and calculated sediment/basement interface (SBI) temperatures along seismic line GeoB00-457 running across Rattlesnake Ridge and south of Zona Bare outcrop (location shown in Figure 19). Symbols and nomenclature as in Figure 4. (a) Seismic data and calculated isotherms. Seismic acquisition and processing discussed by *Zühlsdorff et al.* [2005]. (b) Heat flux data and conductive model calculations. (c) Estimated SBI temperatures. Heat flux is generally 180–200 mW/m^2 across and near Rattlesnake Ridge and appear to be dominantly conductive, whereas heat flux is highly elevated adjacent to Zona Bare outcrop. Because the seismic line does not cross Zona Bare outcrop, it is difficult to evaluate thermal conditions within the edifice, but basement temperatures may be somewhat lower than the typical regional value of 60–65°C. Zona Bare appears to be a site of focused hydrothermal discharge, based on both thermal data and recovery of highly altered pore fluids and clams during RetroFlux coring operations.

mixed (flow-through and local) convection in basement.

[45] Two-dimensional, two-edifice simulations are used to explore free flow between widely separated basement outcrops (Figure 21), including conditions necessary to establish a hydrothermal siphon to maintain circulation. The model domain in these simulations has dimensions of 50 and 5 km, (width and height), with an exposed basement edifice on each end of the model grid, and node spacing of

Table 2. System Properties Used in Numerical Models[a]

Model Property	Sediments	Basement
Porosity ϕ	$\phi = 0.81\ z^{-0.088}$	0.02–0.15
Thermal conductivity λ, W/m-K	$\lambda = \lambda_w^{\phi}\lambda_g^{(1-\phi)}$ $\lambda_w = 0.62$, $\lambda_g = 3.0$	1.70–2.05
Permeability k, m^2	$k = 10^{-18}e^5$	10^{-9}–10^{-17}
Grain density, kg/m^3	2650	2700
Grain specific heat, J/kg-K	800	800
Aquifer thickness, m	NA	100–600

[a] Sediment and basement properties based on field observations and laboratory experiments, as summarized and referenced in the text.

20–500 m. In consideration of symmetry, half of each basalt edifice is represented in the model domain. With a two-dimensional representation of basement relief, the simulated edifices are modeled as infinite ridges (extending into and out of the page) rather than the quasi-conical features seen in the field. More realistic representation of system geometries will require creation of three-dimensional grids, which have yet to be developed for ridge-flank hydrothermal systems. Results from radial and two-dimensional simulations will help to guide creation of future models.

[46] Basal heat flux is 180 mW/m^2 at the lower thermal boundary in all simulations, consistent with the local background heat flux seen on 3.4–3.6 Ma seafloor away from locations of high basement relief in the field area, so that model output and heat flux observations can be compared. Additional modeling constraints are provided by basement fluid pressures and temperatures determined during drilling and long-term borehole monitoring experiments, and fluid flow rates estimated from thermal and geochemical data [e.g., *Davis and Becker*, 2002, 2004; *Elderfield et al.*, 1999; *Fisher et al.*, 1997, 2003a; *Shipboard Scientific Party*, 1997d]. The seafloor boundary condition is free flow for fluid, with pressure and temperature held at hydrostatic and 2°C, respectively. Side boundary conditions are no flow for both fluid and heat. Sediment properties (porosity, density, thermal conductivity, heat capacity, perme-

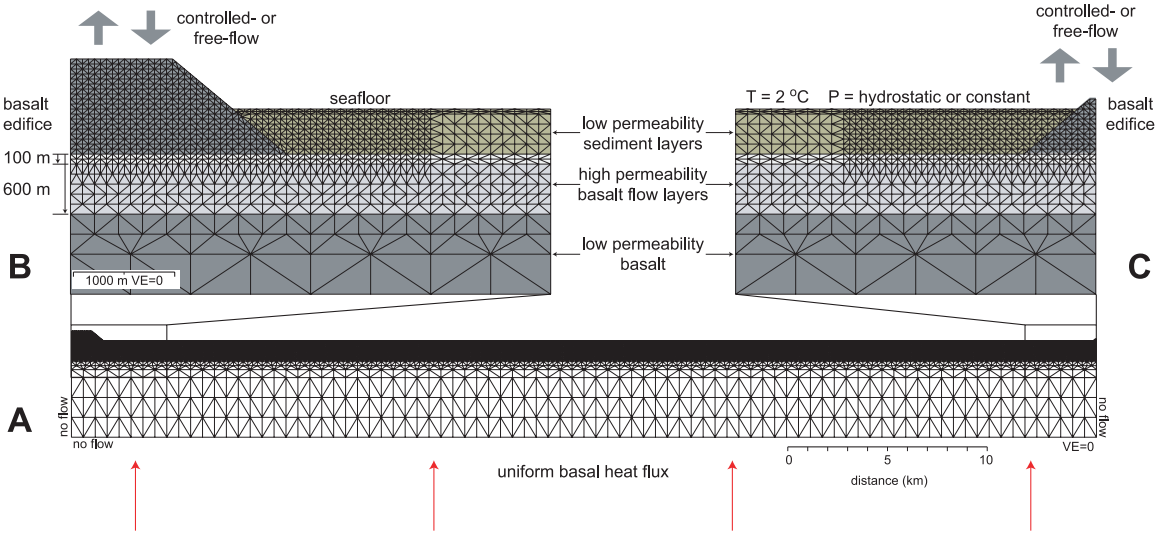

Figure 21. Model domain for simulations of coupled fluid-heat flow. VE, vertical exaggeration. (a) Complete model domain for dual-outcrop simulations illustrating layering of system. The geometry of the partly buried edifices is based on interpretation of seismic data that cross Baby Bare and Grizzly Bare outcrops, which indicate a typical edifice slope of ~35°. Single outcrop radial simulations use either the left or right halves of the grid to replicate conditions around Grizzly Bare and Baby Bare edifices, respectively, with the axis of symmetry running through the center of the respective outcrops. (b) Detail of region within and around the larger basement edifice. (c) Detail of region within and around the smaller outcrop. Single-outcrop models were run conductively, using a high-*Nu* proxy for local convection, and with fluid forced into or out of the grid along the far-field boundary. Dual-outcrop models allowed fluid to recharge and discharge freely through permeable basement after establishing a hydrothermal siphon.

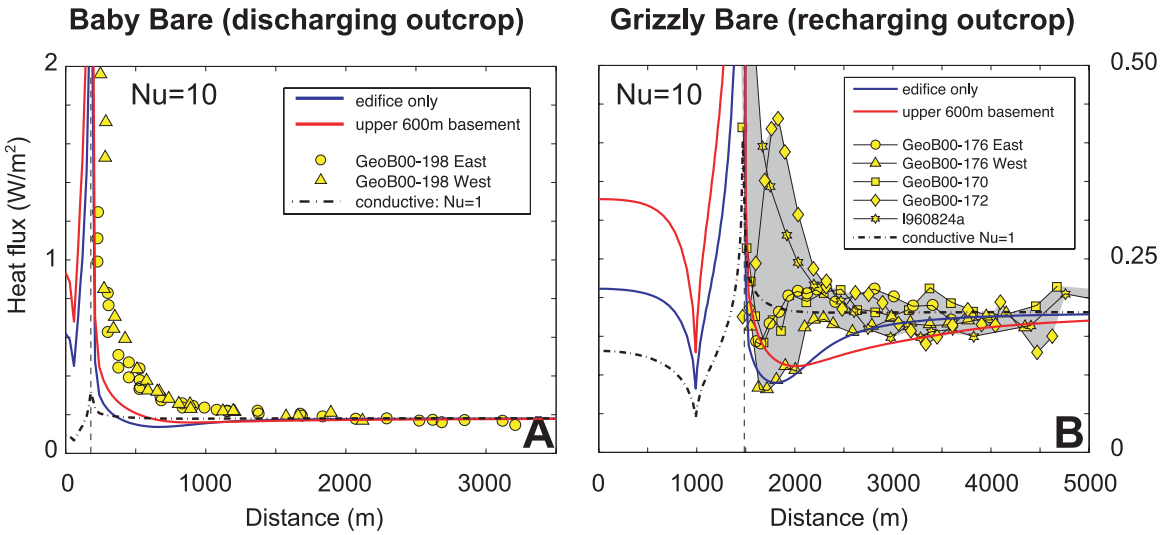

Figure 22. Results of conductive and high-*Nu* simulations of conditions near Baby Bare and Grizzly Bare outcrops compared to seafloor heat flux observations adjacent to the outcrops. Data adjacent to Baby Bare outcrop along seismic line GeoB00-198 are aligned along the outcrop edges, positions for which are indicated with dashed vertical lines. Seafloor heat flux co-located along other seismic transects across Baby Bare outcrop display a similar pattern and are not shown for illustrative purposes. Data adjacent to Grizzly Bare outcrop along seismic lines 960824a, GeoB00-170, -172, and 176, with all data aligned at the outcrop edge. Black dash-dotted lines in all profiles are purely conductive solutions, $Nu = 1$. (a) Comparison of heat flux observations and results of Baby Bare outcrop simulations with $Nu = 10$. Solid curves represent simulations in which the high *Nu* was assigned to different parts of the upper crust, as labeled. Note development of a low heat flux moat around the outcrop. (b) Comparison of heat flux observations and results of Grizzly Bare outcrop simulations with $Nu = 10$. Note that the heat flux moat is deeper and wider in Grizzly Bare outcrop simulations than in Baby Bare outcrop simulations having the same *Nu*, because the larger Grizzly Bare outcrop refracts more heat. Both the amplitude and width of the modeled heat flux profiles scale directly with *Nu*. Neither conductive nor high-*Nu* conditions will replicate heat flux patterns adjacent to Baby Bare and Grizzly Bare outcrops.

ability, storativity) are assigned on the basis of in-situ data and laboratory measurements made on cored material [e.g., *Giambalvo et al.*, 2000; *Shipboard Scientific Party*, 1997d; *Spinelli et al.*, 2004a]. Basement properties are varied within ranges consistent with observations and results of earlier models [e.g., *Becker and Davis*, 2004; *Davis et al.*, 1997c, 2000; *Fisher*, 1998, 2005; *Spinelli and Fisher*, 2004; *Stein and Fisher*, 2003].

5.2. Conductive and High-Nusselt Number Proxy Model Results

[47] The first set of conductive models simulate the distribution of seafloor heat flux adjacent to individual outcrops, allowing quantitative assessment of the extent of thermal anomalies that could result from conductive thermal refraction or vigorous local circulation. Initial simulations use thermal conductivity values typical for sediment and basement found in the field area; additional simulations represent the redistribution of heat associated with vigorous, local convection in basement with a high Nusselt number (*Nu*) proxy [e.g., *Davis et al.*, 1997c; *Fisher and Von Herzen*, 2005; *Spinelli and Fisher*, 2004]. *Nu* is the ratio of total heat transport by convection and conduction to that which would be transported by conduction alone. We simulate this by increasing thermal conductivity within the convecting layer. $Nu = 1$ for purely conductive conditions, whereas *Nu* is much larger when local convection is vigorous.

[48] When conditions are purely conductive, refraction around a basalt edifice generates a small seafloor heat flux anomaly near the edge of basement exposure (Figure 22). A basement edifice the size of Baby Bare outcrop generates an anomaly of $\leq$75 mW/m^2 within tens of meters of the outcrop, whereas the anomaly associated with an edifice the size of Grizzly Bare outcrop is $\leq$225 mW/m^2 within 400 m of the edge of exposed basement. High-*Nu* simulations result in the formation of a higher-amplitude heat flux anomaly immediately adjacent to the outcrop, but also lead to formation of a region of low heat flux farther form the outcrop. This heat flux "moat" is both deeper and more restricted laterally if only the edifice

has a higher *Nu* (conductivity being kept normal in the rest of basement), whereas the moat is shallower and broader when upper basement has a higher *Nu* as well. Both the amplitude and width of the heat flux anomaly scale with increasing *Nu*. Observed heat flux measurements around Baby Bare outcrop are inconsistent with both conductive and high-*Nu* simulations, which fail to replicate the extent of the observed heat flux high adjacent to the outcrop, or (in the case of high-*Nu* simulations) predict a heat flux moat that is not observed (Figure 22a). Heat flux measurements around Grizzly Bare outcrop are more variable, but the conductive and high-*Nu* simulations generally fail to replicate observations around this feature as well. The models are not capable of generating a region of low heat flux that extends only 200–500 m from the outcrop edge (Figures 12 and 13); high-*Nu* simulations generate a heat flux moat that is deeper and/or broader than observed (Figure 22b). Simulations in which $Nu = 10$ only within the basalt edifice are best at reproducing the observed seafloor heat flux profile along seismic line GeoB00-176 west of Grizzly Bare outcrop, but even in this case the moat is broader than observed.

[49] Collectively these simulations suggest that neither conduction nor local convection alone can explain the seafloor thermal patterns seen adjacent to Baby Bare and Grizzly Bare outcrops. This result contrasts significantly with that at sealed-basement sites [e.g., *Davis et al.*, 1997c; *Fisher and Von Herzen*, 2005; *Spinelli and Fisher*, 2004], where a high-*Nu* proxy reasonably replicates heat transport processes in basement. This result is readily explained if heat flux patterns around Baby Bare and Grizzly Bare outcrops result more from the through-flow of hydrothermal fluid and less from the local redistribution of heat by convection [*Fisher et al.*, 2003a; *Mottl et al.*, 1998; *Wheat et al.*, 2004]. The former process can move considerable quantities of heat laterally across kilometers to tens of kilometers, whereas the latter process tends to make lateral heat transport at these scales less efficient [*Davis et al.*, 1999; *Langseth and Herman*, 1981; *Rosenberg et al.*, 2000]. The conductive and high-*Nu* simulations also illustrate the influence of outcrop size on heat flux patterns: larger outcrops create larger thermal anomalies as a result of thermal refraction, particularly if there is local convection in basement, as shown later in fully coupled models.

5.3. Coupled Model Results

5.3.1. Forced-Flow Radial Models

[50] In coupled Baby Bare outcrop models, fluid is forced into the upper 100–600 m of basement at the far domain boundary. Injected fluid has an initial temperature of 2°C, but the fluid warms quickly to ambient conditions, and often becomes isothermal if permeability is sufficiently high as to allow local convection, after a few hundred meters of travel toward the exposed edifice. In Grizzly Bare models, fluid is withdrawn from the upper 100–600 m of basement along the far boundary at ambient (formation) temperature, and 2°C fluid is allowed to recharge through the exposed basalt edifice. In both sets of models, permeability in the upper basement aquifer is varied from 10^{-15} to 10^{-11} m^2. Models with higher permeabilities are difficult to run because of extreme rates of fluid exchange between high-permeability basalt and the overlying ocean, requiring very small time steps and leading to numerical instabilities. As shown later, coupled radial models with permeability higher than 10^{-11} m^2 do not appear to be required to replicate first-order seafloor heat flux patterns near the outcrops.

[51] Coupled models of fluid flow toward Baby Bare outcrop better replicate observed seafloor heat flux patterns than do conductive or high-*Nu* simulations (Figure 23). When basement permeability is 10^{-15} m^2, a fluid flow rate of 50 L/s through the upper 600 m of basement provides the best fit, but thinner aquifers having higher basement permeability also produce seafloor heat flux values similar to those observed (Figure 23). When basement permeability is 10^{-13} to 10^{-12} m^2, unstable secondary convection (periodicity $\sim$ 10 kyr) within and near the edifice results in a range of transient seafloor heat flux patterns that bracket observations, but secondary convection stabilizes for aquifer permeability of 10^{-11} m^2, resulting in a heat flux pattern similar to that seen in the high-*Nu* conductive simulations. A heat flux moat begins to develop at 0.5–2.0 km from the outcrop, inconsistent with observations (Figure 23f). Secondary convection was suppressed in simulations with aquifer permeability of 10^{-15} m^2 (Figure 23b), but these simulations required enormous forcing pressures to drive fluid toward the basement outcrop, suggesting that higher aquifer permeability and limited mixed convection are more realistic in this setting.

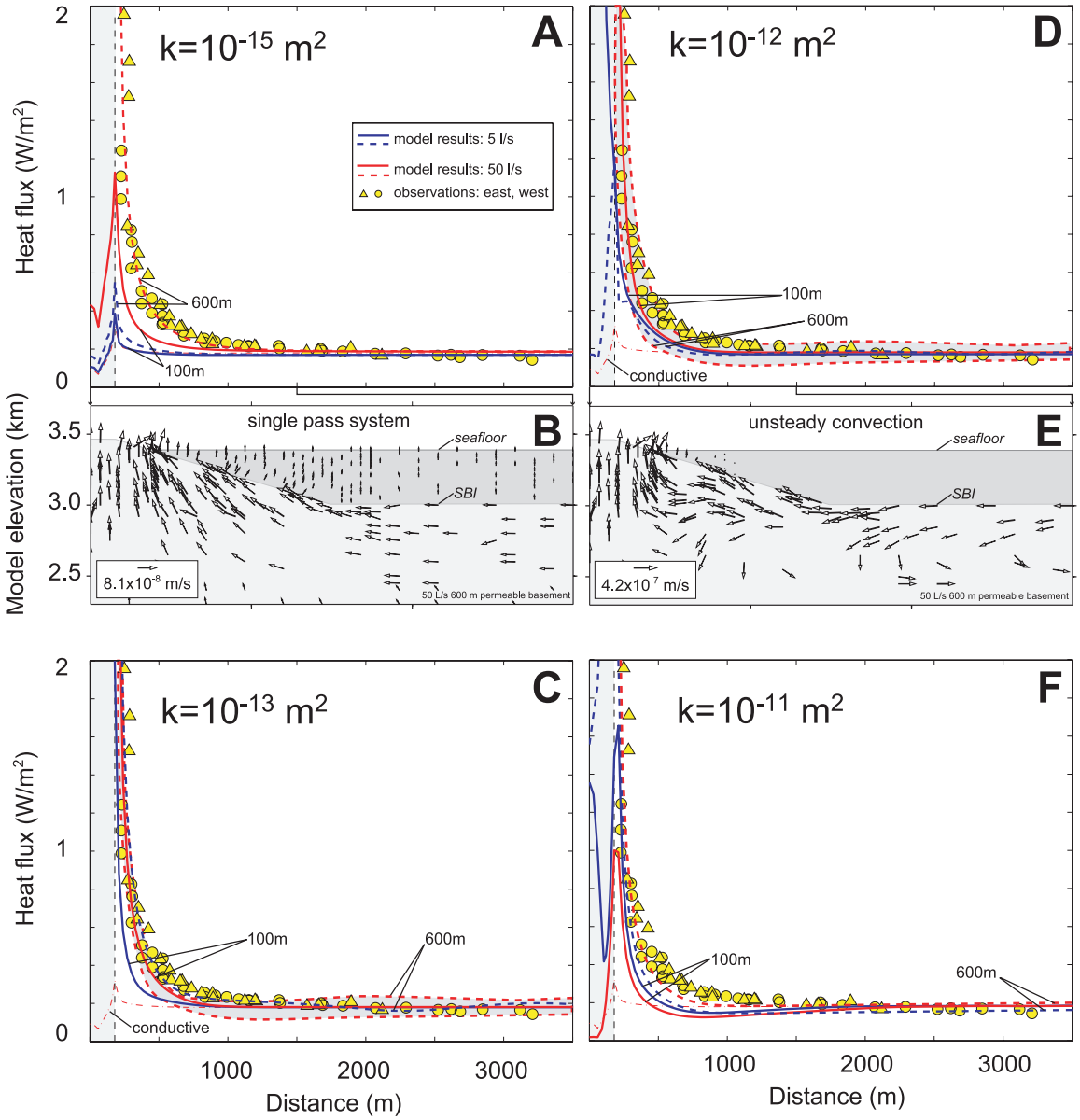

Figure 23. Results from fully coupled numerical models of Baby Bare outcrop. Symbols are the same as in Figure 22. Fluid was pushed into the model domain at the far boundary at 5 and 50 L/s (blue and red curves, respectively), through the upper 100–600 m of basement (solid and dashed curves, respectively), including the basalt edifice. (a) Upper basement permeability is 10^{-15} m^2. (b) Randomly picked subset of lognormalized flow vectors within 1.5 km of the outcrop, showing a single-pass flow system. (c) Upper basement permeability is 10^{-13} m^2. Convection was unstable, leading to a range of heat flux values near the outcrop, as shown with shaded band. (d) Upper basement permeability is 10^{-12} m^2. Convection was unstable, leading to a range of heat flux values near the outcrop, as shown with shaded band. (e) Random subset of lognormalized flow vectors, showing unstable convection in permeable basement. (f) Upper basement permeability is 10^{-11} m^2. Convection stabilizes but becomes so efficient it homogenizes temperatures locally, creating a heat flux moat near the outcrop, as seen in the high-*Nu* simulations (Figure 22).

[52] Coupled models of fluid flow away from Grizzly Bare outcrop provide similar broad constraints on flow rates and bulk crustal properties (Figure 24). Basement aquifer permeability of 10^{-15} m^2 and a recharge rate of 20 L/s can match the general seafloor heat flux pattern along the western side of seismic line GeoB00-176, but the heat flux low near the outcrop is broader than observed (Figure 24a). Basement aquifer permeability of 10^{-13} to 10^{-12} m^2 allows formation of

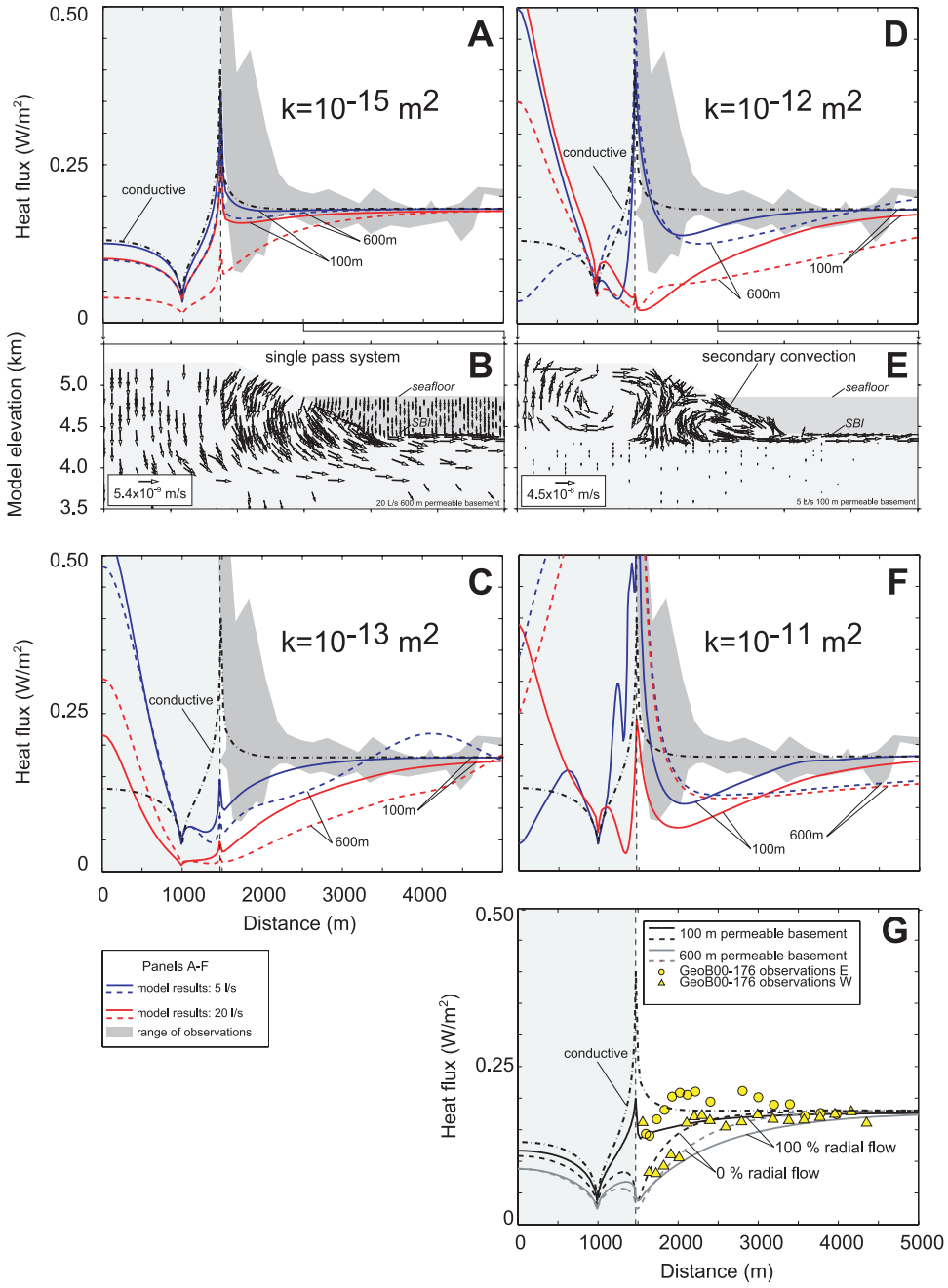

Figure 24. Results from fully coupled numerical models of Grizzly Bare outcrop. Symbols are the same as in Figure 22. Fluid was forced out of the model domain at the far boundary at 5 and 20 L/s (blue and red curves, respectively), through the upper 100–600 m of basement (solid and dashed curves, respectively). (a) Upper basement permeability is 10^{-15} m^2. (b) Randomly picked subset of normalized flow vectors within 3 km of the outcrop, showing a single-pass flow system. (c) Upper basement permeability is 10^{-13} m^2. (d) Upper basement permeability is 10^{-12} m^2. (e) Randomly picked subset of normalized flow vectors, showing secondary convection. (f) Upper basement permeability is 10^{-11} m^2. Secondary convection is so efficient it homogenizes temperatures locally, creating a heat flux moat near the outcrop, as seen in the high-*Nu* simulations (Figure 22). Grizzly Bare outcrop simulations best replicate first-order heat flux patterns near the outcrop when secondary convection is suppressed, although secondary convection helps to replicate local variations along some profiles. (g) Upper basement permeability is 10^{-15} m^2 and recharging fluid is removed at the base of the basement aquifer immediately below the edifice, representing heterogeneous flow pathways (e.g., fluid does not flow radially away from the outcrop). When only the upper 100 m of basement is permeable, this results in a narrower region of low heat flux near the outcrop, more closely approximating conditions along seismic line GeoB00-176 and some other profiles.

secondary convection cells (Figure 24e), particularly at lower fluid recharge rates, which may help to explain some local variability in heat flux at distances of 1–4 km from the Grizzly Bare edifice (Figures 12–15). As around Baby Bare outcrop, aquifer permeability of 10^{-11} m^2 allows secondary convection within and around Grizzly Bare outcrop to become so efficient that the coupled model output resembles that from high-*Nu* simulations (Figure 22f). These simulations include development of heat flux moats that are both deeper and broader than those observed along any survey transects near Grizzly Bare outcrop (Figures 24c and 24d).

[53] The heat flux lows generated near the Grizzly Bare outcrop in these models result from two processes: the recharge of cool water into basement and the flow of this water away from the outcrop toward the far domain boundary. In an effort to separate these effects, we ran an additional set of simulations in which fluid sinks were placed at depth below the outcrop, so that recharging cold fluid could enter and cool the edifice, but would not cool the surrounding basement except by conduction. Although this flow geometry cannot apply everywhere around a recharging outcrop (the recharging water has to flow somewhere), it may represent conditions that would be seen around much of the outcrop as a result of non-radial fluid transport away from the edifice, perhaps along faults or other highly permeable channels. The absence of rapid lateral flow away from the recharging outcrop allows development of a deeper, narrower heat flux low near the outcrop, and is more consistent with observations along seismic line GeoB00-176 (Figure 24g).

5.3.2. Free-Flow Two-Dimensional Models

[54] Free-flow simulations were run with a variety of permeability distributions and initial conditions. In a first set of simulations, initial conditions are conductive and cold hydrostatic (2°C water) or ambient hydrostatic (fluid pressures calculated by vertical boot-strapping based on fluid density under conductive thermal conditions), and the permeability of the outcrops is homogeneous. These models fail to develop outcrop-to-outcrop circulation paths because each outcrop functioned independently to provide sites of both recharge and discharge, at the base and top, respectively, as seen in other single-outcrop free-flow simulations [*Harris et al.*, 2004]. This result is not surprising: development of a hydrothermal siphon necessary to push fluid rapidly across tens of kilometers of the upper crust requires (1) that there be very little energy loss during vertical transport in and out of the primary crustal aquifer and (2) that secondary convection be suppressed within recharging and discharging water columns so that they can remain largely isothermal and the greatest possible pressure difference can develop between the two outcrops and drive a hydrothermal siphon [*Fisher*, 2004; *Fisher et al.*, 2003a; *Stein and Fisher*, 2003].

[55] All subsequent models were run with a single column of highly permeable (10^{-9} m^2) basalt penetrating through the basement outcrops, at the edges of the domain, and connecting to the horizontal basement aquifer at depth. Permeability within the remainder of the outcrops and the basement aquifer is varied to determine what bulk values are consistent with free-flow convection between the two outcrops. Fluid discharge through Baby Bare outcrop is strongly guided by a subvertical normal fault that cuts across the edifice [*Becker et al.*, 2000; *Mottl et al.*, 1998; *Wheat et al.*, 2004]. The significance of faults or other pathways in guiding fluid flow within Grizzly Bare outcrop is unknown, but within heterogeneous crustal systems in general it is likely that most of the fluid flow occurs within a small fraction of the rock [e.g., *Fisher and Becker*, 2000; *Spinelli and Fisher*, 2004].

[56] Once highly permeable vertical channels were included in the models, free-flow convection from outcrop to outcrop developed if permeability within the basement aquifer separating the outcrops was sufficiently high: $\geq 10^{-12}$ m^2 for a 600 m basement aquifer, $\geq 10^{-11}$ m^2 for a 100 m basement aquifer (Figure 25). However, free-flow models started from cold or ambient hydrostatic conditions went from the smaller to the larger outcrop, a direction of flow opposite to that inferred from Grizzly Bare to Baby Bare outcrops. This occurred because conductive refraction was greatest around the larger outcrop, resulting in greater upwarping of isotherms and the formation of a site of hydrothermal discharge. To generate a flow pattern from the larger to the smaller outcrop, we started a suite of two-outcrop simulations with fluid forced to flow in this direction. Once pressure and temperature conditions were established by forced flow, forcing was discontinued and fluid was allowed to circulate freely.

[57] Free flow models having basement aquifer permeability of 10^{-9} m^2 in the upper 600–100 m result in differential pressures at the base of cool and warm water columns of 24–33 kPa driving

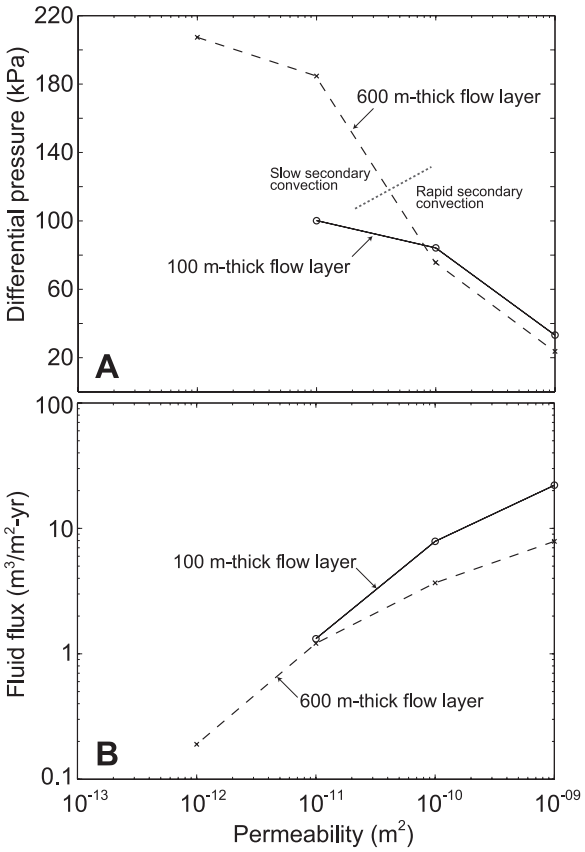

Figure 25. Basement differential pressures at the base of the basement aquifer and fluid fluxes between recharging and discharging outcrops in free-flow simulations. (a) Differential pressures plotted as a function of basement permeability, with curves for 100 and 600 m thick aquifers. Dotted line indicates boundary in 600 m aquifer simulations between rapid and slow secondary convection in basement. (b) Fluid flux versus basement aquifer permeability for models in which free flow between outcrops was sustained. In all cases, flow was forced initially from the larger outcrop to the smaller outcrop. Flow continued along this direction in all simulations marked except for that in which basement permeability was 10^{-12} m^2 in the upper 600 m, for which the flow direction reversed during the simulation.

fluid fluxes of 8–22 m/yr, respectively (Figure 25). The temperature of recharging fluid within the Grizzly Bare edifice is 2–9°C to the depth of the basement aquifer, and the temperature of the discharging fluid is only 20–30°C (Figure 26). This temperature is broadly consistent with temperatures of seafloor seeps surveyed at Baby Bare outcrop, but basement temperatures at depth must be considerably greater, on the order of 60–65°C based on borehole and regional thermal measurements and the chemistry of recovered crustal fluids [*Elderfield et al.*, 1999; *Fisher et al.*, 1997; *Wheat et al.*, 2000]. Modeled upper basement temperatures of 20–30°C result from lateral flow in basement being too rapid to allow the fluid to warm during passage between recharging to discharging edifices.

[58] When basement aquifer permeability between the outcrops is 10^{-10} m^2 in the upper 600–100 m, the differential pressure across the domain is 76–84 kPa, driving fluid fluxes of 4–8 m/yr (Figure 25). Local convection maintains nearly isothermal conditions within much of the basement aquifer, with characteristic temperatures of 38–54°C. Basement aquifer permeability of 10^{-11} m^2 results in differential pressure of 100–185 kPa and a fluid flux near 1 m/yr. Basement temperatures along much of the flow path are 60–65°C, essentially identical to values measured and inferred around the SO, SR, and NO areas. There is still slow, local convection in these simulations, particularly within and near the larger outcrop, but it is too sluggish to homogenize basement aquifer temperatures.

[59] The lowest basement aquifer permeability capable of sustaining outcrop-to-outcrop convection at a lateral length scale of 50 km is 10^{-12} m^2, but only when the aquifer was 600 m thick. When the basement aquifer having this permeability is 100 m thick, flow can not be sustained from the larger to the smaller outcrop. Instead, the flow direction reverses during the simulation, stabilizing with a flow geometry in which the smaller outcrop recharges and the larger outcrop discharges. When the basement aquifer is 600 m thick, discharge through the smaller outcrop is maintained at a fluid flux of 0.2 m/yr, in combination with a differential pressure of 210 kPa and an upper basement temperature of 70°C.

[60] There are significant differences in the discharge temperatures predicted during these simulations for thicker and thinner basement aquifers (Figure 26). In simulations that sustain free-flow convection between the outcrops, where basement permeability is 10^{-11} to 10^{-9} m^2, simulations having a thicker basement aquifer have lower discharge temperatures. This was surprising at first, since the thicker aquifer simulations penetrate deeper into the crust and have lower lateral fluid fluxes; one might expect that slowly moving fluid within a thicker aquifer would have a greater opportunity to mine heat from deeper in the crust and would be warmer. However, fluid mass fluxes are considerably higher in simulations with a thicker aquifer, resulting in a larger volume of cold fluid being recharged. Because the heat capacity of

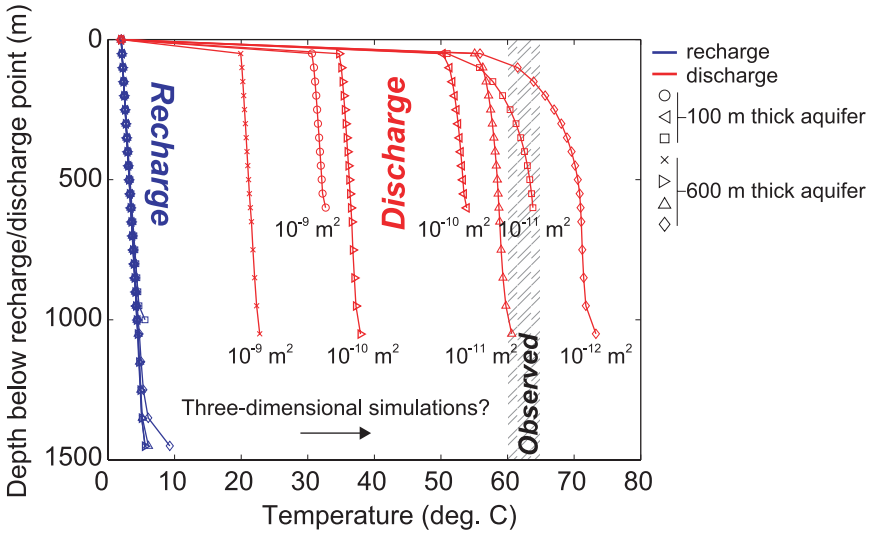

Figure 26. Basement temperature profiles along the highly permeable recharge and discharge conduits at the centers of the edifices (edges of the model domain) for free flow outcrop-to-outcrop simulations. Observed and inferred upper basement temperatures of 60–65°C in the Second Ridge area shown by hatched vertical band. Recharge profiles are similar in all cases, with temperatures of 2–9°C within the edifice and the basement aquifer, but there are significant differences in discharge temperatures. When basement aquifer permeability is 10^{-9} m^2, rapid lateral flow is so efficient at removing heat that upper basement and discharge temperatures never rise above 20–30°C. In contrast, flow rates are lower in simulations with basement aquifer permeability of 10^{-11} m^2, and upper basement and discharge temperatures are 60–65°C, more consistent with observations. It is likely that a higher aquifer permeability would be required for any given discharge temperature profile in a three-dimensional simulation.

seawater is so large, the increase in fluid temperature is lower in thicker aquifers. It is important to remember that one can not consider relations between driving forces, flow rates, and fluid temperatures in terms of cause and effect within a free-flow system. These three parameters develop together within the system in such as way so as to mine heat from the crust as efficiently as possible. This is another reason why these coupled processes must be simulated with a transient model [e.g., *Stein and Fisher*, 2003; *Spinelli and Fisher*, 2004].

6. Discussion and Conclusions

[61] Bathymetric, seismic, and heat flux surveys near basement outcrops on the eastern flank of the JFR provide compelling evidence for the influence of volcanic edifices on fluid transport through the surrounding crust. Data from the Hydrothermal Transition (HT) and First Ridge (FR) areas at the western end of the survey region demonstrate that much of the upper crust is hydrothermally cooled, probably as a result of fluid flow both across and along structural strike. Data from the Second Ridge (SR) area, at the eastern end of the survey region, demonstrate that upper basement remains relatively isothermal across a broad area, and that local background heat flux values may be somewhat lower (by 15–20%) than predicted by standard conductive models for cooling oceanic lithosphere. One might interpret lower seafloor heat flux in this area to indicate that heat is extracted advectively from basement over a broad scale, but this explanation is inconsistent with the lack of spatial trends and regional extent of the observed anomaly. Relatively isolated basement outcrops in this area are sites of focused hydrothermal discharge, but unlike the HT area to the west where there is considerably more basement exposure, the thermal influence of SR outcrops does not appear to extend laterally beyond a few hundred meters from the edifices. It is also possible that the anomaly results from spatial bias in available data, or use of the wrong lithospheric reference. Resolving this dilemma will require collection of limited additional data from this region, co-located on seismic data to avoid areas of significant basement relief, far from basement outcrops.

[62] Recent surveys have also elucidated basement relief, sediment thickness and thermal conditions in two additional parts of this ridge flank, the Southern Outcrop (SO) and Northern Outcrop (NO) areas, ~50 km south and north of the SR area, respectively. The SO area includes two basement

edifices, Grizzly Bare and Grinnin' Bare outcrops. Seismic and thermal data collected radially adjacent to Grizzly Bare outcrop are more variable than those seen adjacent to Baby Bare outcrop, but are highly indicative of hydrothermal recharge. Thermal and geochemical evidence and hydrologic calculations suggest that some of the fluid recharging Grizzly Bare outcrop transits 50 km north before discharging at Baby Bare outcrop. Other fluid recharging at Grizzly Bare outcrop may exit the seafloor at Grinnin' Bare outcrop or elsewhere regionally, although thermal data collected on profiles between recharging and discharging outcrops are limited.

[63] The NO area contains one previously unidentified basement edifice, Zona Bare outcrop. Limited data preclude a detailed understanding of hydrogeologic conditions at depth within and around this feature, but thermal measurements around the outcrop suggest that it is a site mainly of hydrothermal discharge. The source of fluid that sustains discharge at Zona Bare outcrop is unknown, but there are no known areas of basement exposure closer than the SR area.

[64] Radial and two-dimensional numerical models were created to assist in interpretation of hydrogeologic conditions associated with some of these basement outcrops. Single outcrop simulations are conductive or included fixed through-flow rates. Outcrop-to-outcrop models were allowed to flow freely at rates developed dynamically during simulation. A range of basement aquifer permeabilities was tested within different parts of the upper crust, some of which generated results consistent with field observations. Although we must be cautious in using results from idealized models to estimate crustal properties, driving forces, or fluid flow rates, the simulations illustrate how sensitive ridge-flank hydrothermal circulation through outcrops is to selection of appropriate parameters, and suggest that field observations provide important quantitative constraints for these studies.

[65] Radial single outcrop simulations illustrate that conductive and high-*Nu* proxies for local fluid convection in basement are unable to match observed seafloor heat flux patterns adjacent to recharging or discharging outcrops (Figure 22). The passage of fluid through these outcrops, from areas of recharge to discharge, appears to be required to explain the observed heat flux patterns. Models that include discharge of 5–50 L/s of fluid from Baby Bare outcrop through the upper 100–600 m of basement do replicate observed seafloor heat flux patterns, but only if rapid local convection is suppressed in the surrounding crust (Figure 23). When basement permeability is 10^{-11} m^2, local convection results in formation of a heat flux moat around the discharging outcrop, a pattern common to high-*Nu* simulations that is not observed in the field. Higher basement permeabilities would enhance this effect.

[66] Radial single outcrop simulations are less successful in replicating conditions adjacent to a larger, recharging outcrop like Grizzly Bare. Seafloor heat flux patterns predicted with conductive and high-*Nu* simulations are generally inconsistent with observations, generating heat flux moats around the outcrop that are deeper and wider than observed, although simulations with $Nu = 10$ within just the basalt edifice are more consistent with one heat flux profile (Figure 22b). Fully coupled, forced-flow simulations of a recharging outcrop suggest that local convection may help to explain small-scale variations in seafloor heat flux adjacent to the edifice (Figure 24e), and that heterogeneities in flow paths may help to explain why some radial heat flux profiles indicate narrow regions of low heat flux that extend only a few hundred meters from the outcrop (Figure 24g). Once again, bulk crustal permeabilities higher than 10^{-11} m^2 appear to be precluded by the lack of a broad heat flux moat adjacent to Grizzly Bare outcrop.

[67] Free-flow simulations between Grizzly Bare and Baby Bare outcrops include narrow, high-permeability, subvertical conduits through the basement outcrops. These conduits allow vertical fluid flow to be rapid enough so as to maintain a significant differential pressure between sites of hydrothermal recharge and discharge, establishing a hydrothermal siphon [e.g., *Fisher et al.*, 2003a; *Stein and Fisher*, 2001a]. Highly permeable zones may be associated with high-angle normal faults that bound and cut through the abyssal hills upon which Grizzly Bare and Baby Bare outcrops are constructed [*Becker et al.*, 2000; *Mottl et al.*, 1998; *Wheat et al.*, 2000, 2004]. It is necessary to start these simulations with a brief period of forced flow, rather than cold or ambient hydrostatic conditions, in order to initiate the hydrothermal siphon and get fluid circulating in a direction consistent with field observations, from Grizzly Bare to Baby Bare outcrop. The larger outcrop generates a stronger refractive thermal anomaly under conductive conditions and thus tends to become a site of hydrothermal discharge unless the opposite flow pattern

is imposed initially. Once sufficiently rapid fluid flow is initiated and thermal conditions in basement adjust accordingly, this flow is readily maintained without forcing provided that the basement aquifer is sufficiently thick and permeable. It is not clear how one would replicate geologically reasonable initial conditions in order to produce a model that spontaneously produces flow in the observed direction between larger (recharging) and smaller (discharging) outcrops; such a model would presumably begin with crustal formation at the ridge, including magmatism and faulting, and would include subsequent sedimentation (and more limited magmatic and tectonic processes) as the ridge flank ages.

[68] Free-flow simulations suggest that there is a narrow range of basement aquifer thickness, bulk crustal permeability, driving forces, and flow rates that are consistent with observational constraints. Bulk crustal permeability must be $\geq 10^{-12}$ m^2 in order to sustain rapid lateral fluid flow between outcrops separated by 50 km. Upper basement temperatures on the order of 60–65°C, as observed and inferred in the field area [e.g., *Davis and Becker*, 2002; *Davis et al.*, 1992, 1997c; *Fisher et al.*, 1997; *Wheat and Mottl*, 1994], can be produced with models having upper crustal permeability of 10^{-10} to 10^{-11} m^2; basement permeability of 10^{-9} m^2 results in a much lower basement temperature, only 20–30°C. The lowering of upper basement temperatures associated with this extremely high flow rate would result in an enormous (>50%) regional seafloor heat flux anomaly that has not been observed.

[69] The relatively young ^{14}C age of basement fluids nearby Baby Bare outcrop, 4.3 kyr [*Elderfield et al.*, 1999], provide an additional modeling constraint. Actual upper crustal fluid velocities are likely to be much greater than indicated by simple plug-flow consideration of this fluid age because of a combination of flow channeling and diffusive and dispersive losses of fluid youth during transit [*Fisher*, 2004; *Fisher et al.*, 2003a; *Stein and Fisher*, 2003]. Plug flow calculations suggest transit between Grizzly Bare and Baby Bare outcrops at ~10 m/yr, a rate similar to that simulated when upper basement permeability was 10^{-9} to 10^{-10} m^2, but this must be a lower limit on actual fluid velocities.

[70] A lateral basement permeability of 10^{-11} to 10^{-10} m^2 is perhaps most consistent with observational constraints from the area around Baby Bare and Grizzly Bare outcrops. This value is sufficiently high so as to generate upper basement fluid temperatures of 60–65°C, and implies a correction factor of 10–100 to estimate actual basement fluid age from ^{14}C observations. The lower end of this permeability range is consistent with the lack of high-*Nu* convection adjacent to basement outcrops, which would generate deep, broad heat flux moats around basement outcrops. Some numerical models and interpretations of crustal responses to tidal and tectonic perturbations have suggested that effective basement permeabilities could be as high as 10^{-9} m^2, but these estimates are based on other field sites and/or other flow geometries from those simulated in the present study [*Davis and Becker*, 2002, 2004; *Davis et al.*, 1997c, 2000; *Spinelli and Fisher*, 2004; *Stein and Fisher*, 2001a]. In addition, there are issues of measurement scale and assumptions inherent in various methods that remain to be resolved [*Becker and Davis*, 2003; *Davis and Becker*, 2004; *Fisher*, 1998, 2004].

[71] Relations between upper basement temperatures and basement permeabilities may shift somewhat in three-dimensional simulations relative to two-dimensional simulations (Figure 26). Three-dimensional simulations are likely to require somewhat higher basement permeabilities, because they will be less efficient in mining heat on a regional basis than are two-dimensional simulations, but this prediction remains to be tested. It is always difficult to use idealized models (one-dimensional, two-dimensional, or even three-dimensional) to estimate fluxes, driving forces, or basement permeabilities. At best, modeling studies help to illustrate scales of crustal processes and properties that are broadly consistent with observations. These studies also help to elucidate system sensitivity to differences in properties, and to guide future data collection. As observational data sets and models continue to improve, particularly with regard to spatial and temporal complexity, these two distinct approaches will slowly converge, and will continue to help researchers determine actual hydrogeololgic conditions within ridge-flank hydrothermal aquifers.

Acknowledgments

[72] Much of the heat-flux data included in this work was acquired with instrumentation provided under a collaborative program with the Pacific Geoscience Centre, Geological Survey of Canada. Funding and support for this research were provided by grants from the National Science Foundation (OCE98-19242) and the Institute for Geophysics and Planetary Physics (IGPP/LANL Project 1317). This research used data provided by the Ocean Drilling Program (ODP). The ODP is

sponsored by the U.S. National Science Foundation (NSF) and participating countries under the management of Joint Oceanographic Institutions (JOI) Inc. Funding for this research was also provided by a Schlanger Ocean Drilling Fellowship, part of the NSF-sponsored U.S. Science Support Program (USSSP) to ODP. Landmark Graphics and Seismic Micro Technology provided seismic processing and interpretation software. This manuscript was improved by discussions with E. Davis and careful reviews by R. Harris and L. Christiansen.

References

Anderson, R., and M. Hobart (1976), The relation between heat flow, sediment thickness, and age in the Eastern Pacific, *J. Geophys. Res.*, *81*, 2968–2989.

Becker, K., and E. Davis (2003), New evidence for age variation and scale effects of permeabilities of young oceanic crust from borehole thermal and pressure measurements, *Earth. Planet. Sci. Lett.*, *210*, 499–508.

Becker, K., and E. Davis (2004), In situ determinations of the permeability of the igneous oceanic crust, in *Hydrogeology of the Oceanic Lithosphere*, edited by E. E. Davis and H. Elderfield, pp. 189–224, Cambridge Univ. Press, New York.

Becker, K., and A. Fisher (2000), Permeability of upper oceanic basement on the eastern flank of the Endeavor Ridge determined with drill-string packer experiments, *J. Geophys. Res.*, *105*(B1), 897–912.

Becker, N. C., C. G. Wheat, M. J. Mottl, J. Karsten, and E. E. Davis (2000), A geological and geophysical investigation of Baby Bare, locus of a ridge flank hydrothermal system in the Cascadia Basin, *J. Geophys. Res.*, *105*(B10), 23,557–23,568.

Currie, R. G., D. S. Seemann, and R. Riddihough (1982), Total magnetic field anomaly, offshore British Columbia, Geol. Surv. of Can., Sydney, British Columbia, Canada.

Davis, E. E., and K. Becker (2002), Observations of natural-state fluid pressures and temperatures in young oceanic crust and inferences regarding hydrothermal circulation, *Earth. Planet. Sci. Lett.*, *204*, 231–248.

Davis, E. E., and K. Becker (2004), Observations of temperature and pressure: Constraints on ocean crustal hydrologic state, properties, and flow, in *Hydrogeology of the Oceanic Lithosphere*, edited by E. E. Davis and H. Elderfield, pp. 225–271, Cambridge Univ. Press, New York.

Davis, E. E., and R. G. Currie (1993), Geophysical observations of the northern Juan de Fuca Ridge system: Lessons in seafloor spreading, *Can. J. Earth Sci.*, *30*, 278–300.

Davis, E. E., and C. R. B. Lister (1977), Heat flow measured over the Juan de Fuca Ridge: Evidence for widespread hydrothermal circulation in a highly heat-transportive crust, *J. Geophys. Res.*, *82*, 4845–4860.

Davis, E. E., D. S. Chapman, C. Forster, and H. Villinger (1989), Heat-flow variations correlated with buried basement topography on the Juan de Fuca Ridge flank, *Nature*, *342*, 533–537.

Davis, E. E., et al. (1992), FlankFlux: An experiment to study the nature of hydrothermal circulation in young oceanic crust, *Can. J. Earth Sci.*, *29*(5), 925–952.

Davis, E. E., D. S. Chapman, H. Villinger, S. Robinson, J. Grigel, A. Rosenberger, and D. Pribnow (1997a), Seafloor heat flow on the eastern flank of the Juan de Fuca Ridge: Data from the "FlankFlux" studies through 1995, *Proc. Ocean Drill. Program Initial Rep.*, *168*, 23–33.

Davis, E. E., A. T. Fisher, and J. Firth (1997b), *Proceedings of the Ocean Drilling Program, Initial Reports*, vol. 168, 470 pp., Ocean Drill. Program, College Station, Tex.

Davis, E. E., K. Wang, J. He, D. S. Chapman, H. Villinger, and A. Rosenberger (1997c), An unequivocal case for high Nusselt-number hydrothermal convection in sediment-buried igneous oceanic crust, *Earth. Planet. Sci. Lett.*, *146*, 137–150.

Davis, E. E., D. S. Chapman, K. Wang, H. Villinger, A. T. Fisher, S. W. Robinson, J. Grigel, D. Pribnow, J. Stein, and K. Becker (1999), Regional heat-flow variations across the sedimented Juan de Fuca Ridge eastern flank: Constraints on lithospheric cooling and lateral hydrothermal heat transport, *J. Geophys. Res.*, *104*(B8), 17,675–17,688.

Davis, E. E., K. Wang, K. Becker, and R. E. Thomson (2000), Formation-scale hydraulic and mechanical properties of oceanic crust inferred from pore-pressure response to periodic seafloor loading, *J. Geophys. Res.*, *105*(B6), 13,423–13,435.

Elderfield, H., C. G. Wheat, M. J. Mottl, C. Monnin, and B. Spiro (1999), Fluid and geochemical transport through oceanic crust: A transect across the eastern flank of the Juan de Fuca Ridge, *Earth. Planet. Sci. Lett.*, *172*, 151–165.

Fisher, A. (2004), Rates and patterns of fluid circulation, in *Hydrogeology of the Oceanic Lithosphere*, edited by E. E. Davis and H. Elderfield, pp. 339–377, Cambridge Univ. Press, New York.

Fisher, A. T. (1998), Permeability within basaltic oceanic crust, *Rev. Geophys.*, *36*(2), 143–182.

Fisher, A. T. (2005), Marine hydrogeology: Future prospects for major advances, *Hydrol. J.*, *13*, 69–97, doi:10.1007/s10040-004-0400-y.

Fisher, A. T., and K. Becker (2000), Channelized fluid flow in oceanic crust reconciles heat-flow and permeability data, *Nature*, *403*, 71–74.

Fisher, A. T., K. Becker, and E. E. Davis (1997), The permeability of young oceanic crust east of Juan de Fuca Ridge determined using borehole thermal measurements, *Geophys. Res. Lett.*, *24*, 1311–1314.

Fisher, A. T., E. E. Davis, and C. Escutia (2000), *Proceedings of the Ocean Drilling Program*, *Science Results*, vol. 168, 185 pp., Ocean Drill. Program, College Station, Tex.

Fisher, A. T., et al. (2003a), Hydrothermal recharge and discharge across 50 km guided by seamounts on a young ridge flank, *Nature*, *421*, 618–621.

Fisher, A. T., C. A. Stein, R. N. Harris, K. Wang, E. A. Silver, M. Pfender, M. Hutnak, A. Cherkaoui, R. Bodzin, and H. Villinger (2003b), Abrupt thermal transition reveals hydrothermal boundary and role of seamounts within the Cocos Plate, *Geophys. Res. Lett.*, *30*(11), 1550, doi:10.1029/2002GL016766.

Fisher, A. T., and R. P. Von Herzen (2005), Models of hydrothermal circulation within 106 Ma seafloor: Constraints on the vigor of fluid circulation and crustal properties, below the Madeira Abyssal Plain, *Geochem. Geophys. Geosyst.*, *6*, Q11001, doi:10.1029/2005GC001013.

Fisher, A. T., T. Urabe, and A. Klaus (2005a), *Proceedings of the IODP: Expedition Reports*, vol. 301, Integrated Ocean Drill. Program, College Station, Tex.

Fisher, A. T., et al. (2005b), Scientific and technical design and deployment of long-term, subseafloor observatories for hydrogeologic and related experiments, IODP Expedition 301, eastern flank of Juan de Fuca Ridge, in *Proceedings of the IODP*, vol. 301, edited by A. T. Fisher, T. Urabe, and A. Klaus, Integrated Ocean Drill. Program, College Station, Tex.

Giambalvo, E., A. T. Fisher, L. Darty, J. T. Martin, and R. P. Lowell (2000), Origin of elevated sediment permeability in a hydrothermal seepage zone, eastern flank of Juan de Fuca Ridge, and implications for transport of fluid and heat, *J. Geophys. Res.*, *105*(B1), 913–928.

Harris, R. N., A. T. Fisher, and D. Chapman (2004), Fluid flow through seamounts and implications for global mass fluxes, *Geology*, *32*(8), 725–728, doi:10.1130/G20387.1.

Jacobson, R. S. (1992), Impact of crustal evolution on changes of the seismic properties of the uppermost oceanic crust, *Rev. Geophys.*, *30*, 23–42.

Johnson, H. P., K. Becker, and R. P. V. Herzen (1993), Near-axis heat flow measurements on the northern Juan de Fuca Ridge: Implications for fluid circulation in oceanic crust, *Geophys. Res. Lett.*, *20*(17), 1875–1878.

Kappel, E. S., and W. B. F. Ryan (1986), Volcanic episodicity and a non-steady state rift valley along the northeast pacific spreading centers: Evidence from sea marc I, *J. Geophys. Res.*, *91*(B14), 13,925–13,940.

Karsten, J., N. C. Becker, M. J. Mottl, and C. G. Wheat (1998), Petrology of Baby Bare and Mama Bare lavas, *Geophys. Res. Lett.*, *25*(1), 117–120.

Karsten, J. L., S. R. Hammond, E. E. Davis, and R. G. Currie (1986), Detailed geomorphology and neotectonics of the Endeavour segment, Juan de Fuca Ridge: New results from Seabeam swath mapping, *Geol. Soc. Am. Bull.*, *97*, 213–221.

Langseth, M. G., and B. Herman (1981), Heat transfer in the oceanic crust of the Brazil Basin, *J. Geophys. Res.*, *86*, 10,805–10,819.

Langseth, M. G., R. D. Hyndman, K. Becker, S. H. Hickman, and M. H. Salisbury (1984), The hydrogeological regime of isolated sediment ponds in mid-oceanic ridges, *Initial Rep. Deep Sea Drill. Proj.*, *78B*, 825–837.

Lister, C. R. B. (1970), Heat flow of the Juan de Fuca Ridge, *J. Geophys. Res.*, *75*, 2648–2654.

Lister, C. R. B. (1977), Qualitative models of spreading center processes, including hydrothermal penetration, *Tectonophysics*, *37*, 203–218.

Marescotti, P., D. A. Vanko, and R. Cabella (2000), From oxidizing to reducing alteration: Mineralogical variations in pillow basalts from the east flank, Juan de Fuca Ridge, *Proc. Ocean Drill. Program Sci. Results*, *168*, 119–136.

Mottl, M. J., and C. G. Wheat (1994), Hydrothermal circulation through mid-ocean ridge flanks: Fluxes of heat and magnesium, *Geochim. Cosmochim. Acta*, *58*, 2225–2237.

Mottl, M. J., et al. (1998), Warm springs discovered on 3.5 Ma oceanic crust, eastern flank of the Juan de Fuca Ridge, *Geology*, *26*, 51–54.

Parsons, B., and J. G. Sclater (1977), An analysis of the variation of ocean floor bathymetry and heat flow with age, *J. Geophys. Res.*, *82*, 803–829.

Press, W. H., B. P. Flannery, S. A. Teukolsky, and W. T. Vetterling (1989), *Numerical Recipes: The Art of Scientific Computing*, 702 pp., Cambridge Univ. Press, New York.

Pribnow, D. F. C., E. E. Davis, and A. T. Fisher (2000), Borehole heat flow along the eastern flank of the Juan de Fuca Ridge, including effects of anisotropy and temperature dependence of sediment thermal conductivity, *J. Geophys. Res.*, *105*(B6), 13,449–13,456.

Rosenberg, N., A. T. Fisher, and J. Stein (2000), Large-scale lateral heat and fluid transport in the seafloor: Revisiting the well-mixed aquifer model, *Earth. Planet. Sci. Lett.*, *182*, 93–101.

Rosenberger, A., E. E. Davis, and H. Villinger (2000), Data report: Hydrocell-95 and -96 single-channel seismic data on the eastern Juan de Fuca Ridge flank, *Proc. Ocean Drill. Program, Sci. Results*, *168*, 9–19.

Shipboard Scientific Party (1997a), Buried Basement Transect (Sites 1028, 1029, 1030, 1031, and 1032), *Proc. Ocean Drill. Program Initial Rep.*, *168*, 161–214.

Shipboard Scientific Party (1997b), Scientific Party, Hydrothermal Transition Transect (Sites 1023, 1024, and 1025), *Proc. Ocean Drill. Program Initial Rep.*, *168*, 49–100.

Shipboard Scientific Party (1997c), Introduction and summary: Hydrothermal circulation in the oceanic crust and its consequences on the eastern flank of the Juan de Fuca Ridge, *Proc. Ocean Drill. Program Initial Rep.*, *168*, 7–21.

Shipboard Scientific Party (1997d), Rough Basement Transect (Sites 1026 and 1027), *Proc. Ocean Drill. Program Initial Rep.*, *168*, 101–160.

Siegel, S. (1956), *Nonparametric Statistics for the Behavioral Sciences*, 279 pp., McGraw-Hill, New York.

Smith, W. H. F., and D. T. Sandwell (1997), Global sea floor topography from satellite altymetry and ship depth soundings, *Science*, *277*, 1956–1962.

Spinelli, G. A., and A. T. Fisher (2004), Hydrothermal circulation within topographically rough basaltic basement on the Juan de Fuca Ridge flank, *Geochem. Geophys. Geosyst.*, *5*, Q02001, doi:10.1029/2003GC000616.

Spinelli, G. A., E. G. Giambalvo, and A. T. Fisher (2004a), Hydrologic properties and distribution of sediments, in *Hydrogeology of the Oceanic Lithosphere*, edited by E. E. Davis and H. Elderfield, pp. 151–188, Cambridge Univ. Press, New York.

Spinelli, G. A., L. Zühlsdorff, A. T. Fisher, C. G. Wheat, M. Mottl, V. Spieß, and E. R. Giambalvo (2004b), Hydrothermal seepage patterns above a buried basement ridge, eastern flank of the Juan de Fuca Ridge, *J. Geophys. Res.*, *109*, B01102, doi:10.1029/2003JB002476.

Stein, C., and S. Stein (1992), A model for the global variation in oceanic depth and heat flow with lithospheric age, *Nature*, *359*, 123–129.

Stein, J. S., and A. T. Fisher (2001a), Lateral hydrothermal circulation beneath the eastern flank of the Juan de Fuca Ridge: Thermal, chemical and modeling constraints, *Eos Trans AGU*, *82*(47), Fall Meet. Suppl., Abstract S21A-0560.

Stein, J. S., and A. T. Fisher (2001b), Multiple scales of hydrothermal circulation in Middle Valley, northern Juan de Fuca Ridge: Physical constraints and geologic models, *J. Geophys. Res.*, *106*(B5), 8563–8580.

Stein, J. S., and A. T. Fisher (2003), Observations and models of lateral hydrothermal circulation on a young ridge flank: Numerical evaluation of thermal and chemical constraints, *Geochem. Geophys. Geosyst.*, *4*(3), 1026, doi:10.1029/2002GC000415.

Thomson, R. E., E. Davis, and B. J. Burd (1995), Hydrothermal venting and geothermal heating in Cascadia Basin, *J. Geophys. Res.*, *100*, 6121–6141.

Underwood, M., K. D. Hoke, A. T. Fisher, E. G. Giambalvo, E. E. Davis, and L. Zühlsdorff (2005), Provenance, stratigraphic architecture, and hydrogeologic effects of turbidites in northwestern Cascadia Basin, Pacific Oceanz, *J. Sediment. Res.*, *75*(1), 149–164.

Villinger, H., I. Grevemeyer, N. Kaul, J. Hauschild, and M. Pfender (2002), Hydrothermal heat flux through aged oceanic crust: Where does the heat escape?, *Earth. Planet. Sci. Lett.*, *202*(1), 159–170.

Von Herzen, R. P. (2004), Geothermal evidence for continuing hydrothermal circulation in older (>60 Ma) ocean crust, in

Hydrogeology of the Oceanic Lithosphere, edited by E. E. Davis and H. Elderfield, pp. 414–450, Cambridge Univ. Press, New York.

Wheat, C. G., and M. J. Mottl (1994), Hydrothermal circulation, Juan de Fuca Ridge eastern flank: Factors controlling basement water composition, *J. Geophys. Res.*, *99*, 3067–3080.

Wheat, C. G., H. Elderfield, M. J. Mottl, and C. Monnin (2000), Chemical composition of basement fluids within an oceanic ridge flank: Implications for along-strike and across-strike hydrothermal circulation, *J. Geophys. Res.*, *105*(B6), 13,437–13,447.

Wheat, C. G., M. J. Mottl, A. T. Fisher, D. Kadko, E. E. Davis, and E. Baker (2004), Heat flow through a basaltic outcrop on a sedimented young ridge flank, *Geochem. Geophys. Geosyst.*, *5*, Q12006, doi:10.1029/2004GC000700.

Williams, D. L., K. Green, T. H. van Andel, R. P. Von Herzen, J. R. Dymond, and K. Crane (1979), The hydrothermal mounds of the Galapagos Rift: Observations with DSRV Alvin and detailed heat flow studies, *J. Geophys. Res.*, *84*, 7467–7484.

Wilson, D. S. (1993), Confidence intervals for motion and deformation of the Juan de Fuca plate, *J. Geophys. Res.*, *98*(B16), 16,053–16,071.

Zühlsdorff, L., M. Hutnak, A. Fisher, V. Speiss, E. Davis, M. Nedimovic, S. Carbotte, H. Villinger, and K. Becker (2005), Site surveys related to IODP Expedition 301: Image-Flux (SO149) and RetroFlux (TN116) expeditions and earlier studies, *Proc. Ocean Drill. Program Sci.*, 301.

Zyvoloski, G. A., B. A. Robinson, Z. D. Dash, and L. L. Trease (1996), Users manual for the FEHMN application, Los Alamos Natl. Lab., Los Alamos, N. M.